

# Evidence of Odderon-exchange from scaling properties of elastic scattering at TeV energies

T. Csörgő<sup>a,1,2,3</sup>, T. Novák<sup>b,2</sup>, R. Pasechnik<sup>c,4,5</sup>, A. Ster<sup>d,1</sup>, I. Szanyi<sup>e,1,6</sup>

<sup>1</sup>Wigner FK, H-1525 Budapest 114, POB 49, Hungary

<sup>2</sup>EKU KRC, H-3200 Gyöngyös, Mátrai út 36, Hungary

<sup>3</sup>CERN, CH-1211 Geneva 23, Switzerland

<sup>4</sup>Department of Astronomy and Theoretical Physics, Lund University, SE-223 62 Lund, Sweden

<sup>5</sup>Nuclear Physics Institute ASCR, 25068 Řež, Czech Republic

<sup>6</sup>Eötvös University, H - 1117 Budapest, Pázmány P. s. 1/A, Hungary

the date of receipt and acceptance should be inserted later

**Abstract** We study the scaling properties of the differential cross section of elastic proton-proton ( $pp$ ) and proton-antiproton ( $p\bar{p}$ ) collisions at high energies. We introduce a new scaling function, that scales – within the experimental errors – all the ISR data on elastic  $pp$  scattering from  $\sqrt{s} = 23.5$  to 62.5 GeV to the same universal curve. We explore the scaling properties of the differential cross-sections of the elastic  $pp$  and  $p\bar{p}$  collisions in a limited TeV energy range. Rescaling the TOTEM  $pp$  data from  $\sqrt{s} = 7$  TeV to 2.76 and 1.96 TeV, and comparing it to D0  $p\bar{p}$  data at 1.96 TeV, our results provide an evidence for a  $t$ -channel Odderon exchange at TeV energies, with a significance of at least  $6.26\sigma$ .

## 1 Introduction

One of the most important and critical tests of quantum chromodynamics (QCD) in the infrared regime is provided by the ongoing studies of elastic differential hadron-hadron scattering cross section at various energies and momentum transfers. The characteristics of the elastic amplitude, its both real and imaginary parts, carry a plenty of information about the inner proton structure, the proton profile in the impact parameter space and its energy dependence, as well as about the properties of QCD exchange interaction at low momentum transfers.

The first and most precise measurements of the total, elastic and differential cross sections of elastic  $pp$  collisions, together with the  $\rho$ -parameter, has recently been performed

by the TOTEM Collaboration at the Large Hadron Collider (LHC) at CERN at the highest energy frontier of  $\sqrt{s} = 13$  TeV (for the corresponding recent TOTEM publications, see Refs. [1–4]). A correct theoretical interpretation of the LHC data, together with the lower-energy Tevatron and ISR data, is a subject of intense debates and ongoing research development in the literature, see e.g. Refs. [5, 6]. Among the important recent advances, the recent data by the TOTEM Collaboration for the first time have indicated the presence of an odd-under-crossing (or C-odd) contribution to the elastic scattering amplitude known as the Odderon [7]. In particular, a comparison of the differential cross-section of elastic proton-proton  $pp$  scattering obtained by the TOTEM Collaboration at  $\sqrt{s} = 2.76$  TeV with D0 results on elastic proton-antiproton  $p\bar{p}$  scattering at 1.96 TeV [8] indicates important qualitative differences that can be attributed to the Odderon effect [4, 9]. In more rigorous language of QCD, an Odderon exchange is usually associated with a quarkless odd-gluon (e.g. three-gluon, to the lowest order) bound state such as a vector glueball, and a vast literature is devoted to theoretical understanding of its implications. An increase of the total cross section,  $\sigma_{\text{tot}}(s)$ , associated with a decrease of the real-to-imaginary ratio,  $\rho(s)$ , with energy, first identified at  $\sqrt{s} = 13$  TeV [1, 2], also indicated a possible Odderon effect.

The TOTEM measurements have recently triggered intense theoretical studies in the literature. In particular, the Phillips-Barger parameterisation of the elastic amplitude has been found to describe the recent  $pp$  data in Refs. [10, 11]. Several other Regge parameterisations have also been found to describe the LHC data reasonably well (see e.g. Refs. [6, 12, 13]), while the Pomeron dominance has been explored in a generic Regge theory set-up in Refs. [14, 15]. In Ref. [5], a new feature of the second diffractive cone in the differential cross-section of elastic scattering at large  $t$  and  $s$  has

<sup>a</sup>e-mail: tcsorgo@cern.ch

<sup>b</sup>e-mail: novak.tamas@uni-eszterhazy.hu

<sup>c</sup>e-mail: roman.pasechnik@thep.lu.se

<sup>d</sup>e-mail: ster.andras@wigner.mta.hu

<sup>e</sup>e-mail: istvan.szanyi@cern.ch

been identified arguing about the existence of two stationary points in  $d\sigma/dt$  at the LHC energies and relating those to the two-scale structure of protons at these energies. Remarkably, this rules out the dominance of perturbative exchanges of a few non-interacting gluons pointing towards a core-like proton substructure found also in the framework of the so-called Lévy imaging technique in Refs. [9, 16]. For a thorough discussion of general properties of the  $s$ -dependence of  $\rho(s)$  in the light of the TOTEM data and its connections to the growing energy dependence of the elastic-to-total cross-sections ratio, see Ref. [17]. A number of studies based upon a QCD-based analysis of the Odderon signatures considering the non-linear QCD evolution have also been triggered recently (see e.g. Refs. [18–21]).

Important statements about the maximal nature of the Odderon effect were made in Refs. [6, 22–24] but apparently these studies still lack a rigorous statistical significance analysis. Although the  $s$ -dependence of both  $\sigma_{\text{tot}}(s)$  and  $\rho(s)$  is consistent with an Odderon effect, this indication is not a unique Odderon signal as the same effect can also be attributed to the secondary Reggeon effects [18], reinforcing the elusiveness of the Odderon. As it was argued in Ref. [25] any conclusions about the magnitude of the Odderon effects based upon the  $\rho(s)$  measurement alone have to be made with special care due to a zero in the real part of the elastic amplitude at very small  $t$ , as the latter can affect the Coulomb-nuclear interference region at high energies.

In earlier studies of Refs. [26, 27], the Odderon signatures have been identified and qualitatively described in a model-independent way using the power of the Lévy imaging technique [9]. One of such signatures concern the presence of a dip-and-bump structure in the differential cross section of elastic  $pp$  collisions and the lack of such a structure in elastic  $p\bar{p}$  collisions. The latter effectively emerges in the  $t$ -dependence of the elastic slope  $B(t)$ , that crosses zero for elastic  $pp$  collisions and remains non-negative for all values of  $t$  in elastic  $p\bar{p}$  collisions. Besides, Ref. [9] noted that the position of the node of the nuclear phase  $\phi(t)$ , as reconstructed with the help of the Lévy expansion method, is characteristically and qualitatively different for elastic  $pp$  from  $p\bar{p}$  collisions, thus, indicating the Odderon exchange. In addition, the presence of a smaller substructure of the proton has been revealed in the data that is imprinted in the behaviour of the  $t$ -dependent elastic slope  $B(t)$ , apparent at large values of  $t$ . In particular, in Refs. [9, 16, 26, 27] two substructures of two distinct sizes has been identified in the low (a few tens of GeV) and high (a few TeV) energy domains, respectively. Besides, a new statistically significant feature in the  $b$ -dependent shadow (or inelasticity) profile has been found at the maximal available energy  $\sqrt{s} = 13$  TeV and represents a long-debated hollowness, or “black-ring” effect that emerges instead of the conventionally anticipated “black-disk” regime [16, 26].

In this paper, in order to further unveil the important characteristics of elastic hadron-hadron scattering we study the scaling properties of the existing data sets available from the ISR and Tevatron colliders as well as those provided by the TOTEM Collaboration in a TeV energy range [1–4, 28]. We investigate a generic scaling behavior of elastic differential proton-(anti)proton scattering cross section, with the goal of transforming out the trivial colliding energy dependent variation of the key observables like that of the total and elastic cross-sections  $\sigma_{\text{tot}}(s)$  and  $\sigma_{\text{el}}(s)$ , the elastic slope  $B(s)$  and the real-to-imaginary ratio  $\rho(s)$ . We search successfully for a universal scaling function and the associated data-collapsing behaviour that is valid not only in the low- $|t|$  domain, but also in the dip-and-bump region. We discuss the physics implications of such a scaling behaviour and explore its consequences for understanding of the Odderon effect as well as the high-energy behaviour of the proton structure.

The paper is organised as follows. In section 2, we recapitulate the formalism that is utilized for evaluation of the observables of elastic proton-(anti)proton scattering in the TeV energy range. In section 3, we connect this formalism to a more general strategy of the experimental Odderon search, namely, to the search for a crossing-odd component in the differential cross-section of elastic proton-(anti)proton scattering. In section 4, we study some of the scaling functions of elastic scattering already existing in the literature as well as propose a new scaling function denoted as  $H(x)$  that is readily measurable in  $pp$  and  $p\bar{p}$  collisions, and present a first test of the  $H(x)$  scaling in the ISR energy range of 23.5 – 62.5 GeV. Subsequently, in section 5 we extend these studies to the TeV (Tevatron and LHC) energy range, where the possible residual effects of Reggeon exchange are expected to be below the scale of the experimental errors [29]. In section 6, we present a method of how to quantify the significance of our findings, giving the formulas that are used to evaluate  $\chi^2$ , confidence level (CL), and significance in terms of the standard deviation,  $\sigma$ . Appendix A details the robustness and symmetry properties of the  $\chi^2$  definition and provide the final significance of at least 6.26  $\sigma$ . In section 7, we discuss how to employ the newly found scaling behavior of the differential cross-section in the search for an Odderon effect. In section 8, we present further, more detailed results of our studies with the help of  $H(x)$  and compare such a scaling function for  $pp$  differential cross-sections at the LHC energies with the  $p\bar{p}$  scaling function at the Tevatron energy. In section 9 we evaluate the significance of the Odderon-effect, and find that it is at least a 6.26 $\sigma$ -significant effect. Subsequently, we present several cross-checks in section 10 and discuss the main results in section 11. Finally, we summarize and conclude our work in section 12.

## 2 Formalism

For the sake of completeness and clarity, let us start first with recapitulating the connection between the scattering amplitude and the key observables of elastic scattering, following the conventions of Refs. [30–33].

The Mandelstam variables  $s$  and  $t$  are defined as usual  $s = (p_1 + p_2)^2$ ,  $t = (p_1 - p_3)^2$  for an elastic scattering of particles  $a$  and  $b$  with incoming four-momenta  $p_1$  and  $p_2$ , and outgoing four-momenta  $p_3$  and  $p_4$ , respectively.

The elastic cross-section is given as integral of the differential cross-section of elastic scattering:

$$\sigma_{\text{el}}(s) = \int_0^\infty d|t| \frac{d\sigma(s, t)}{dt} \quad (1)$$

The elastic differential cross section is

$$\frac{d\sigma(s, t)}{dt} = \frac{1}{4\pi} |T_{\text{el}}(s, \Delta)|^2, \quad \Delta = \sqrt{|t|}. \quad (2)$$

The  $t$ -dependent slope parameter  $B(s, t)$  is defined as

$$B(s, t) = \frac{d}{dt} \ln \frac{d\sigma(s, t)}{dt} \quad (3)$$

and in the experimentally accessible low- $t$  region this function is frequently assumed or found within errors to be a constant. In this case, a  $t$ -independent slope parameter  $B(s)$  is introduced as

$$B(s) \equiv B_0(s) = \lim_{t \rightarrow 0} B(s, t), \quad (4)$$

where the  $t \rightarrow 0$  limit is taken within the experimentally probed region. Actually, experimentally the optical  $t = 0$  point can only be approached by extrapolations from the measurements in various  $-t > 0$  kinematically accessible regions that depend on the optics and various settings of the particle accelerators and colliding beams.

According to the optical theorem, the total cross section is also found by a similar extrapolation. Its value is given by

$$\sigma_{\text{tot}}(s) \equiv 2 \text{Im} T_{\text{el}}(\Delta = 0, s), \quad (5)$$

while the ratio of the real to imaginary parts of the elastic amplitude is found as

$$\rho(s, t) \equiv \frac{\text{Re} T_{\text{el}}(s, \Delta)}{\text{Im} T_{\text{el}}(s, \Delta)} \quad (6)$$

and its measured value at  $t = 0$  reads

$$\rho(s) \equiv \rho_0(s) = \lim_{t \rightarrow 0} \rho(s, t). \quad (7)$$

Here, the  $t \rightarrow 0$  limit is taken typically as an extrapolation in dedicated differential cross section measurements at very

low  $-t$ , where the parameter  $\rho_0$  can be measured using various Coulomb-Nuclear Interference methods. The differential cross section at the optical ( $t = 0$ ) point is thus represented as

$$\left. \frac{d\sigma(s)}{dt} \right|_{t \rightarrow 0} = \frac{1 + \rho_0^2(s)}{16\pi} \sigma_{\text{tot}}^2(s). \quad (8)$$

In the impact-parameter  $b$ -space, we have the following relations:

$$t_{\text{el}}(s, b) = \int \frac{d^2\Delta}{(2\pi)^2} e^{-i\Delta b} T_{\text{el}}(s, \Delta) = \frac{1}{2\pi} \int J_0(\Delta b) T_{\text{el}}(s, \Delta) \Delta d\Delta, \quad (9)$$

$$\Delta \equiv |\Delta|, \quad b \equiv |b|. \quad (10)$$

This Fourier-transformed elastic amplitude  $t_{\text{el}}(s, b)$  can be represented in the eikonal form

$$t_{\text{el}}(s, b) = i \left[ 1 - e^{-\Omega(s, b)} \right], \quad (11)$$

where  $\Omega(s, b)$  is the so-called opacity function (known also as the eikonal function), which is complex in general. The shadow profile function is then defined as

$$P(s, b) = 1 - \left| e^{-\Omega(s, b)} \right|^2. \quad (12)$$

For clarity, let us note that other conventions are also used in the literature and for example the shadow profile  $P(b, s)$  is also referred to as the inelasticity profile function as it corresponds to the probability distribution of inelastic proton-proton collisions in the impact parameter  $b$  with  $0 \leq P(b, s) \leq 1$ . When the real part of the scattering amplitude is neglected,  $P(b, s)$  is frequently denoted as  $G_{\text{inel}}(s, b)$ , see for example Refs. [34–38].

## 3 Looking for Odderon effects in the differential cross-section of elastic scattering

As noted in Refs. [10, 39], the only direct way to see the Odderon is by comparing the particle and antiparticle scattering at sufficiently high energies provided that the high-energy  $pp$  or  $p\bar{p}$  elastic scattering amplitude is a sum or a difference of even and odd C-parity contributions, respectively,

$$T_{\text{el}}^{pp}(s, t) = T_{\text{el}}^+(s, t) + T_{\text{el}}^-(s, t), \quad (13)$$

$$T_{\text{el}}^{p\bar{p}}(s, t) = T_{\text{el}}^+(s, t) - T_{\text{el}}^-(s, t), \quad (14)$$

$$T_{\text{el}}^+(s, t) = T_{\text{el}}^P(s, t) + T_{\text{el}}^f(s, t), \quad (15)$$

$$T_{\text{el}}^-(s, t) = T_{\text{el}}^O(s, t) + T_{\text{el}}^\omega(s, t). \quad (16)$$

where the even-under-crossing part consists of the Pomeron and the  $f$  Reggeon trajectory, while the odd-under-crossing part contains the Odderon and a contribution from the  $\omega$  Reggeon. It is clear from the above formulae that the odd

component of the amplitude can be extracted from the difference of the  $pp$  and  $p\bar{p}$  scattering amplitudes.

At sufficiently high energies, the relative contributions from secondary Regge trajectories are suppressed, as they decay as negative powers of the colliding energy  $\sqrt{s}$ . In Ref. [10], the authors argued that the LHC energy scale is already sufficiently large to suppress the Reggeon contributions, and they presented the  $(s, t)$ -dependent contributions of an Odderon exchange to the differential and total cross-sections at typical LHC energies. More recently, this observation was confirmed in Ref. [29], suggesting that indeed the relative contribution of the Reggeon trajectories is well below the experimental precision in elastic  $pp$  scattering in the TeV energy range. The analysis of Ref. [10] relies on a model-dependent, phenomenological picture formulated in the framework of the Phillips-Barger model [40] and is focused primarily on fitting the dip region of elastic  $pp$  scattering, but without a detailed analysis of the tail and cone regions. In Ref. [29], a phenomenological Reggeon + Pomeron + Odderon exchange model is employed to study, in particular, the possible hollowness effect in the high-energy elastic  $pp$  collisions. More recently, a similar study of the Phillips-Barger model was performed in Ref. [11] using the most recent TOTEM data on elastic  $pp$  scattering. Similarly, Ref. [41] has also argued that the currently highest LHC energy of  $\sqrt{s} = 13$  TeV is sufficiently high to see the Odderon contribution.

In this paper, we follow Refs. [10, 29, 41] and assume that the Reggeon contributions to the elastic scattering amplitudes for  $\sqrt{s} \geq 1.96$  TeV and at higher energies are negligibly small. We search for an odd-under-crossing contribution to the scattering amplitude, in a model independent way, and find that such a non-vanishing contribution is present at a TeV scale that is recognised as an Odderon effect. The vanishing nature of the Reggeon contributions offers a direct way of extracting the Odderon as well as the Pomeron contributions,  $T_{\text{el}}^O(s, t)$  and  $T_{\text{el}}^P(s, t)$ , respectively, from the elastic  $pp$  and  $p\bar{p}$  scattering data at sufficiently high colliding energies as follows

$$T_{\text{el}}^P(s, t) = \frac{1}{2} \left( T_{\text{el}}^{pp}(s, t) + T_{\text{el}}^{p\bar{p}}(s, t) \right) \quad \text{for } \sqrt{s} \geq 1 \text{ TeV}, \quad (17)$$

$$T_{\text{el}}^O(s, t) = \frac{1}{2} \left( T_{\text{el}}^{pp}(s, t) - T_{\text{el}}^{p\bar{p}}(s, t) \right) \quad \text{for } \sqrt{s} \geq 1 \text{ TeV}. \quad (18)$$

These kind of studies rely on the extrapolation of the fitted model parameters of  $pp$  and  $p\bar{p}$  reactions to an exactly the same energy, given that the elastic  $pp$  and  $p\bar{p}$  scattering data have not been measured at the same (or close enough) energies in the TeV region so far. Another problem is a lack of precision data at the low- and high- $|t|$ , primarily, in  $p\bar{p}$  collisions. Recently, the TOTEM Collaboration noted in Ref. [4] that “Under the condition that the effects due to the energy difference between TOTEM and D0 can be neglected, the result” (namely the differential cross-

section measured by TOTEM at  $\sqrt{s} = 2.76$  TeV) “provides evidence for a colourless 3-gluon bound state exchange in the  $t$ -channel of the proton-proton elastic scattering”. In other words, if the effects due to the energy difference between TOTEM and D0 measurements can be neglected, the direct comparison of the differential cross section of elastic  $pp$  scattering at  $\sqrt{s} = 2.76$  with that of  $p\bar{p}$  scattering at  $\sqrt{s} = 1.96$  TeV provides a *conditional* evidence for a colourless three-gluon state exchange in the  $t$ -channel.

In this paper, we show that the conditional evidence stated by TOTEM can be turned to an unconditional evidence, i.e. a discovery of the Odderon, by closing the energy gap as much as possible at present, without a direct measurement, based on a re-analysis of already published TOTEM and D0 data. Here we take the data at a face value as given in published sources and do not attempt to extrapolate any model or model parameters towards their unmeasured values (in unexplored energy domains). Instead, we discuss a new kind of scaling relations, that we test on the experimental data and show their data-collapsing behaviour in a limited energy range. We demonstrate that such a data-collapsing behaviour can be used to close the small energy gap between the highest-energy elastic  $p\bar{p}$  collisions,  $\sqrt{s} = 1.96$  TeV and the lowest-energy elastic  $pp$  collisions at the LHC where the public data are available,  $\sqrt{s} = 2.76$  TeV. We then look for even-under-crossing and odd-under-crossing contributions by comparing the scaling functions of  $pp$  and  $p\bar{p}$  collisions in the TeV energy range. In other words, we look for a robust Odderon signature in the difference of the scaling functions of the elastic differential cross-section between  $pp$  and  $p\bar{p}$  collisions. We thus discuss the Odderon features that can be extracted in a model-independent manner directly by comparing the corresponding data sets to one another.

Let us start with three general remarks as direct consequences of Eqs. (17,18):

- If the Odderon exchange effect is negligibly small (within errors, equal to zero) or if it does not interfere with that of the Pomeron at a given energy, then the differential cross sections of the elastic  $pp$  and  $p\bar{p}$  scattering have to be equal:

$$T_{\text{el}}^O(s, t) = 0 \implies \frac{d\sigma^{pp}}{dt} = \frac{d\sigma^{p\bar{p}}}{dt} \quad \text{for } \sqrt{s} \geq 1 \text{ TeV}. \quad (19)$$

- If the differential cross sections of elastic  $pp$  and  $p\bar{p}$  collisions are equal within the experimental errors, this does not imply that the Odderon contribution has to be equal to zero. Indeed, the equality of cross sections does not require the equality of complex amplitudes:

$$\frac{d\sigma^{pp}}{dt} = \frac{d\sigma^{p\bar{p}}}{dt} \quad \text{for } \sqrt{s} \geq 1 \text{ TeV} \not\Rightarrow T_{\text{el}}^O(s, t) = 0. \quad (20)$$

- If the  $pp$  differential cross sections differ from that of  $p\bar{p}$  scattering at the same value of  $s$  in a TeV energy



domain, then the Odderon contribution to the scattering amplitude cannot be equal to zero, i.e.

$$\frac{d\sigma^{pp}}{dt} \neq \frac{d\sigma^{p\bar{p}}}{dt} \text{ for } \sqrt{s} \geq 1 \text{ TeV} \implies T_{\text{el}}^O(s, t) \neq 0. \quad (21)$$

Such a difference is thus a clear-cut signal for the Odderon-exchange, if the differential cross sections were measured at exactly the same energies. However, currently such data are lacking in the TeV energy range. Our research strategy in this paper is to scale out the known  $s$ -dependencies of the differential cross section by scaling out its dependencies on  $\sigma_{\text{tot}}(s)$ ,  $\sigma_{\text{el}}(s)$ ,  $B(s)$  and  $\rho(s)$  functions. The residual scaling functions will be compared for the  $pp$  and  $p\bar{p}$  elastic scattering to see if any difference remains.

In what follows, we introduce and discuss the newly found scaling function  $H(x)$  in section 4 and subsequently evaluate the significance of these observations as detailed in sections 6 and 9.

#### 4 Possible scaling relations at low values of $|t|$

In this section, let us first investigate the scaling properties of the experimental data based on a simple Gaussian model elaborating on the discussion presented in Ref. [42]. The motivation for this investigation is that we would like to work out a scaling law that works at least in the simplest, exponential diffractive cone approximation, and scales out the trivial  $s$ -dependencies of  $\sigma_{\text{tot}}(s)$ ,  $\sigma_{\text{el}}(s)$ ,  $\rho(s)$ , and  $B(s)$ . Based on the results of such a frequently used exponential approximation, we gain some intuition and experience on how to generalize such scaling laws for realistic non-exponential differential cross sections.

Experimentally, the low- $|t|$  part of the measured distribution is usually approximated with an exponential,

$$\frac{d\sigma}{dt} = A(s) \exp[B(s)t], \quad (22)$$

where it is explicitly indicated that both the normalization parameter  $A \equiv A(s)$  and the slope parameter  $B \equiv B(s)$  are the functions of the center-of-mass energy squared  $s$ . If the data deviate from such an exponential shape, that can be described if one allows for a  $t$ -dependence of the slope parameter  $B \equiv B(s, t)$  as defined in Eq. (3). For simplicity, we would like to scale out the energy dependence of the elastic slope  $B(s) \equiv B(s, t=0)$  from the differential cross section of elastic scattering, together with the energy dependence of the elastic and total cross sections,  $\sigma_{\text{el}}(s)$  and  $\sigma_{\text{tot}}(s)$ , as detailed below. For this purpose, let us follow the lines of a similar derivation in Refs. [29, 42].

It is clear that Eq. (22) corresponds to an exponential “diffractive cone” approximation, that may be valid in the low- $t$  domain only. This equation corresponds to the so called “Grey Gaussian” approximation that suggests a relationship

between the nuclear slope parameter  $B(s)$ , the real-to-imaginary ratio  $\rho_0(s)$ , the total cross section  $\sigma_{\text{tot}}(s)$ , and the elastic cross section  $\sigma_{\text{el}}(s)$  as follows [29, 43, 44]:

$$A(s) = B(s) \sigma_{\text{el}}(s) = \frac{1 + \rho_0^2(s)}{16\pi} \sigma_{\text{tot}}^2(s), \quad (23)$$

$$B(s) = \frac{1 + \rho_0^2(s)}{16\pi} \frac{\sigma_{\text{tot}}^2(s)}{\sigma_{\text{el}}(s)}. \quad (24)$$

Such relations for  $A$  and  $B$  parameters in terms of the elastic and total cross sections are particularly useful when studying the shadow profile function as detailed below. The above relationships, in a slightly modified form, have been utilized by TOTEM to measure the total cross section at  $\sqrt{s} = 2.76, 7, 8$  and  $13$  TeV in Refs. [1, 45–47], using the luminosity independent method. In what follows, we do not suppress the  $s$ -dependence of the observables, i.e.  $\sigma_{\text{tot}} \equiv \sigma_{\text{tot}}(s)$ ,  $\sigma_{\text{el}} \equiv \sigma_{\text{el}}(s)$ .

#### 4.1 Scaling properties of the shadow profiles

In the exponential approximation given by Eqs. (22,23,24), the shadow profile function introduced in Eq. (12) has a remarkable and very interesting scaling behaviour, as anticipated in Ref. [29]:

$$P(b, s) = 1 - \left[ 1 - r(s) \exp\left(-\frac{b^2}{2B(s)}\right) \right]^2 - \rho_0^2(s) r^2(s) \exp\left(-\frac{b^2}{B(s)}\right), \quad (25)$$

$$r(s) \equiv 4 \frac{\sigma_{\text{el}}(s)}{\sigma_{\text{tot}}(s)}. \quad (26)$$

Thus, the shadow profile at the center,  $P_0(s) \equiv P(b=0, s)$  reads as

$$P_0(s) = \frac{1}{1 + \rho_0^2(s)} - [1 + \rho_0^2(s)] \left[ r(s) - \frac{1}{1 + \rho_0^2(s)} \right]^2, \quad (27)$$

which cannot become maximally absorptive (or black), i.e.  $P_0(s) = 1$  is not reached at those colliding energies, where  $\rho_0$  is not negligibly small. The maximal absorption corresponds to  $P_0(s) = \frac{1}{1 + \rho_0^2(s)}$ , which is rather independent of the detailed  $b$ -dependent shape of the inelastic collisions [29]. It is achieved when  $r(s)$  of eq. (26) approaches the value  $r(s) = 1/(1 + \rho_0^2(s))$ . Thus, at such a threshold, we have the following critical value of the ratio

$$\left. \frac{\sigma_{\text{el}}(s)}{\sigma_{\text{tot}}(s)} \right|_{\text{threshold}} = \frac{1}{4 [1 + \rho_0^2(s)]}. \quad (28)$$

As  $\rho_0 \leq 0.15$  for the existing measurements and  $\rho_0(s)$  seems to decrease with increasing energies at least in the  $8 \leq \sqrt{s} \leq 13$  TeV region, the critical value of the elastic-to-total cross section ratio (28) corresponds to, roughly,  $\sigma_{\text{el}}/\sigma_{\text{tot}} \approx 24.5 - 25.0$  %. Evaluating the second derivative of  $P(b, s)$

at  $b = 0$ , one may also observe that it changes sign from a negative to a positive one exactly at the same threshold given by Eq. (28). Such a change of sign can be interpreted as an onset of the hollowness effect [29]. The investigation of such a hollowness at  $b = 0$  is a hotly debated topic in the literature. For early papers on this fundamental feature of  $pp$  scattering at the LHC and asymptotic energies, see Refs. [35, 36, 44, 48–51], as well as Refs. [29, 34, 37, 38, 52–59] for more recent theoretical discussions.

As pointed out in Ref. [42], the threshold (28), within errors, is reached approximately already at  $\sqrt{s} = 2.76$  TeV. The threshold behavior saturates somewhere between 2.76 and 7 TeV and a transition may happen around the threshold energy of  $\sqrt{s_{\text{th}}} \approx 2.76 - 4$  TeV. The elastic-to-total cross section ratio becomes significantly larger than the threshold value at  $\sqrt{s} = 13$  TeV colliding energies. As a result, the shadow profile function of the proton undergoes a qualitative change in the region of  $2.76 < \sqrt{s} < 7$  TeV energies. At high energies, with  $\sigma_{\text{el}} \geq \sigma_{\text{tot}}/4$ , the hollowness effect may become a generic property of the impact parameter distribution of inelastic scatterings. However, the expansion at low impact parameters corresponds to the large- $|t|$  region of elastic scattering, where the diffractive cone approximation of Eqs. (22,23,24) technically breaks down, and more refined studies are necessary (see below). For the most recent, significant and model-independent analysis of the hollowness effect at the LHC and its extraction directly from the TOTEM data, see Ref. [16].

#### 4.2 Scaling functions for testing the black-disc limit

When discussing the scaling properties of the differential cross section of elastic scattering, let us mention that various scaling laws have been proposed to describe certain features and data-collapsing behaviour of elastic proton-proton scattering already in the 1970-s. One of the early proposals was the so called geometric scaling property of the inelastic overlap function [60, 61]. The concept of geometric scaling was based on a negligibly small ratio of the real-to-imaginary part of the scattering amplitude at  $t = 0$ ,  $\rho_0 \leq 0.01$  and resulted in an  $s$ -independent ratio of the elastic-to-total cross-sections,  $\sigma_{\text{el}}/\sigma_{\text{tot}} \approx \text{const}(s)$ , while at the LHC energies,  $\rho_0$  is not negligibly small and the elastic-to-total cross section ratio is a strongly rising function of  $s$ . Here, we just note about the geometric scaling as one of the earliest proposals to have a data-collapsing behavior in elastic scattering, but we look in detail for other kind of scaling laws that are more in harmony and consistency with the recent LHC measurements [42].

Let us first detail the following two dimensionless scaling functions proposed in Ref. [32] and denoted as  $F(y)$  and  $G(z)$  in what follows. These scaling functions were introduced in order to cross-check if elastic  $pp$  collisions at the

LHC energies approach the so-called black-disc limit, expected at ultra-high energies, or not. In a strong sense, the black disc limit corresponds to the shadow profile  $P(b) = \theta(R_b - b)$  that results in  $\sigma_{\text{el}}/\sigma_{\text{tot}} = 1/2$ , independently of the black disc radius  $R_b$ . This limit is clearly not yet approached at LHC energies, but in a weak sense, a black-disc limit is considered to be reached also if the shadow profile function at  $b = 0$  reaches unity, i.e.  $P(b = 0) = 1$ , corresponding to black disc scattering at zero impact parameter. This kind of black disc scattering might have been approached at  $\sqrt{s} = 7$  TeV LHC energy [33].

The first scaling function of the differential cross-section is defined as follows:

$$F(y) = \frac{|t|}{\sigma_{\text{tot}}} \frac{d\sigma}{dt}, \quad (29)$$

$$y = t/\sigma_{\text{tot}}, \quad (30)$$

In the diffractive cone approximation, the  $s$ -dependence in  $F(y)$  does not cancel out but can be approximately written as

$$F(y) \simeq y B(s) \frac{\sigma_{\text{el}}(s)}{\sigma_{\text{tot}}^2(s)} \frac{d\sigma}{dt} \Big|_{t=y/\sigma_{\text{tot}}(s)}, \quad (31)$$

$$B(s)t = y \frac{B(s)}{\sigma_{\text{tot}}(s)}. \quad (32)$$

This result clearly indicates that in the diffractive cone, the  $F(y)$  scaling is strongly violated by the energy-dependent factors, while for a black-disc scattering, the  $F(y)$  scaling has to be valid, see Ref. [32] for more details. Indeed, the aim to introduce the scaling function  $F(y)$  was to clarify that even at the highest LHC energies we do not reach the black-disc limit (in the strong sense). As discussed in the previous section, the deviations from the black-disc limit might be due to the effects of the real part and the hollowness, i.e. reaching a black-ring limit instead of a black-disc one at the top LHC energies.

Since in the  $F(y)$  scaling function the position of the diffractive minimum (dip) remains  $s$ -dependent, yet another scaling function denoted as  $G(z)$  was proposed to transform out such  $s$ -dependence of the dip. This function was introduced also in Ref. [32] as follows:

$$G(z) = \frac{z|t_{\text{dip}}(s)|}{\sigma_{\text{tot}}(s)} \frac{d\sigma}{dt} \Big|_{t=z|t_{\text{dip}}(s)|}, \quad (33)$$

$$z = \frac{t}{|t_{\text{dip}}(s)|}. \quad (34)$$

In principle, all black-disc scatterings, regardless of the value of the total cross section, should show a data-collapsing behaviour to the same  $G(z)$  scaling function. As observed in Ref. [32], such an asymptotic form of the  $G(z)$  scaling function is somewhat better approached at the LHC energies as compared to the lower ISR energies but still not reproduced it exactly. This is one of the key indications the black-disc limit in the elastic  $pp$  scattering is not achieved at the LHC,

up to  $\sqrt{s} = 13$  TeV. This may have several other important implications. For example, this result indicates that in simulations of relativistic heavy-ion collisions at the LHC energies, more realistic profile functions have to be used to describe the impact parameter dependence of the inelastic  $pp$  collisions: a simple gray or black-disc approximation for the inelastic interactions neglects the key features of elastic  $pp$  collisions at the TeV energy scales.

One advantage of the scaling variables  $y$  and  $z$  mentioned above is that they are dimensionless. Numerically,  $G(z)$  corresponds to the  $F(y)$  function if the scaling variable  $y$  is rescaled to  $z$ . As indicated in Fig. 23 of Ref. [32], indeed the main difference between  $F(y)$  and  $G(z)$  is that the diffractive minimum is rescaled in  $G(z)$  to the  $z = 1$  position, so  $G(z)$  has less evolution with  $s$  as compared to  $F(y)$ . However, as it is clear from the above discussion, the function

$$G(z) \simeq \frac{\sigma_{\text{el}}(s)}{\sigma_{\text{tot}}(s)} B(s) z |t_{\text{dip}}(s)| \left. \frac{d\sigma}{dt} \right|_{t=z|t_{\text{dip}}(s)|}, \quad (35)$$

$$B(s)t = B(s)t_{\text{dip}}(s)z, \quad (36)$$

is well-defined only for  $pp$  elastic scattering, where a unique dip structure is observed experimentally.

Even the dip region is not always measurable in  $pp$  reactions if the experimental acceptance is limited to the cone region, which is a sufficient condition for the total cross section measurements. If the acceptance was not large enough in  $|t|$  to observe the diffractive minimum, or, in the case when the diffractive minimum did not clearly exist, then neither the  $F(y)$  nor the  $G(z)$  scaling functions would be usable. So, the major disadvantage of these scaling functions for extracting the Odderon signatures from the data is that in  $p\bar{p}$  collisions no significant diffractive minimum is found by the D0 collaboration at 1.96 TeV [8]. Besides, even if  $z$  variable were defined, the above expressions indicate, in agreement with Fig. 23 of Ref. [32], that the  $G(z)$  scaling function has a non-trivial energy-dependent evolution in the cone ( $z \ll 1$ ) region. Due to these reasons, variables  $z$  and  $y$  are not appropriate scaling variables for a scale-invariant analysis of the crossing-symmetry violations at high energies.

Having recapitulated the considerations in Ref. [42], with an emphasis on the  $s$ -dependence of the parameters, let us now consider, how these  $s$ -dependencies can be scaled out at low values of  $|t|$ , where the diffraction cone approximation is valid, by evaluating the scaling properties of the experimental data on the differential elastic  $pp$  and  $p\bar{p}$  cross sections. For this purpose, let us look into the scaling properties of the differential cross sections and their implications related to the Odderon discovery in a new way.

#### 4.3 A new scaling function for the elastic cone

In the elastic cone region, all the  $pp$  and  $p\bar{p}$  differential cross sections can be rescaled to a straight line in a linear-

logarithmic plot, when the horizontal axis is scaled by the slope parameter to  $-tB(s)$  while the vertical axis is simultaneously rescaled by  $B(s)\sigma_{\text{el}}(s)$ , namely,

$$\frac{1}{B(s)\sigma_{\text{el}}(s)} \frac{d\sigma}{dt} = \exp[tB(s)] \quad \text{versus} \quad x = -tB(s). \quad (37)$$

This representation, in the diffractive cone, scales out the  $s$ -dependencies of the total and elastic cross section,  $\sigma_{\text{tot}}(s)$  and  $\sigma_{\text{el}}(s)$ , and also that of the slope parameter,  $B(s)$ . As a function of the scaling variable  $x = -tB$ , it will correspond to the plot of  $\exp(-x)$  i.e. a straight line with slope  $-1$  on a linear-logarithmic plot. It is well-known that the elastic scattering is only approximately exponential in the diffractive cone, but by scaling out this exponential feature one may more clearly see the scaling violations on this simple scaling plot. We will argue that such a scaling out of the trivial energy-dependent terms can be used as a powerful method in the search for the elusive Odderon effects in the comparison of elastic  $pp$  and  $p\bar{p}$  data in the TeV energy range.

In what follows, we investigate the scaling properties of the new scaling function,

$$H(x) \equiv \frac{1}{B(s)\sigma_{\text{el}}(s)} \frac{d\sigma}{dt}, \quad (38)$$

$$x = -tB(s). \quad (39)$$

This simple function has four further advantages summarized as follows:

1. First of all, it satisfies a sum-rule or normalization condition rather trivially,  $\int dx H(x) = 1$ , as follows from the definition of the elastic cross section.
2. Secondly, if almost all of the elastically scattered particles belong to the diffractive cone, the differential cross-section at the optical point is also given by  $\left. \frac{d\sigma}{dt} \right|_{t=0} = A(s) = B(s)\sigma_{\text{el}}(s)$ , and in these experimentally realized cases we have another (approximate) normalization condition, namely,  $H(0) = 1$ .
3. Third, in the diffractive cone, all the energy dependence is scaled out from this function, i.e.,  $H(x) = \exp(-x)$  that shows up as a straight line on a linear-logarithmic plot with a trivial slope  $-1$ .
4. Last, but not least, the slope parameter  $B(s)$  is readily measurable not only for  $pp$  but also for  $p\bar{p}$  collisions, hence the  $pp$  and the  $p\bar{p}$  data can be scaled to the same curve without any experimental difficulties.

Let us first test these ideas by using the ISR data in the energy range of  $\sqrt{s} = 23.5 - 62.5$  GeV. The results are shown in Fig. 1 which indicates that the ISR data indeed show a data-collapsing behaviour.

At low values of  $x$ , the scaling function is indeed, approximately,  $H(x) \simeq \exp(-x)$ , that remains a valid approximation over, at least, five orders of magnitude in the decrease of the differential cross section. However, at the ISR

energies, the scaling seems to be valid, within the experimental uncertainties, not only at low values of  $x = -Bt$ , but extended to the whole four-momentum transfer region, including the dip and bump region ( $15 \leq x \leq 30$ ) as well. Even at large- $|t|$  after the bump region, corresponding to  $x \geq 30$ , the data can approximately be scaled to the same, non-exponential scaling function:  $H(x) \neq \exp(-x)$  in the tails of the distribution. Thus, Fig. 1 indeed indicates a non-trivial data-collapsing behaviour to the same, non-trivial scaling function at the ISR energy range of  $\sqrt{s} = 23.5 - 62.5$  GeV.

This observation motivated us to generalize the derivation presented above in this section, to arbitrary positively definite non-exponential scaling functions  $H(x)$ . Such a generalisation is performed in the next subsection, in order to give a possible explanation of the data-collapsing behaviour in Fig. 1.

#### 4.4 Generalized scaling functions for non-exponential differential cross-sections

In this section, we search for a novel type of scaling functions of  $pp$  elastic data that may be valid not only in the diffractive cone, but also in the crucial dip and bump region, as well. In Fig. 1, we have noticed that the data-collapsing behaviour may extend well above the small  $x = -tB$  region significantly beyond the diffractive maximum, indicating a clear deviation of the scaling function  $H(x)$  from the exponential shape.

In addition, a recent detailed study of the low- $|t|$  behaviour of the differential elastic  $pp$  cross section at  $\sqrt{s} = 8$  TeV observed a more than  $7\sigma$ -significant deviation from the exponential shape [63, 64], which also corresponds to a non-exponentiality in the scaling function  $H(x)$  even in the low- $|t|$ , or small  $x$ , range.

In this section, we thus further generalize the derivation of the  $H(x) = \exp(-x)$  scaling function, in order to allow for arbitrary positively definite functions with  $H(x=0) = 1$  normalisation, and to develop a physical interpretation of the experimental observations.

Let us start the derivation from the relation of the elastic scattering amplitude in the impact parameter space  $t_{\text{el}}(s, b)$  and the complex opacity function  $\Omega(s, b)$  based on Eq. (11), using the same notation as in Ref. [33]:

$$t_{\text{el}}(s, b) = i \left[ 1 - \exp(-i \text{Im} \Omega(s, b)) \sqrt{1 - \tilde{\sigma}_{\text{in}}(s, b)} \right]. \quad (40)$$

The shadow profile function  $P(s, b)$  is equal to the inelastic scattering profile  $\tilde{\sigma}_{\text{in}}(s, b)$  as follows from Eq. (12),  $P(s, b) = \tilde{\sigma}_{\text{in}}(s, b)$ . The imaginary part of the opacity function  $\Omega$  is generally not known or less constrained by the data, but it is experimentally known that  $\rho_0(s)$  is relatively small at high energies: at all the measured LHC energies and below,  $\rho_0 \leq 0.15$ , hence,  $\rho^2 \leq 2.3\%$ .

Here, we thus follow the choice of Ref. [33], that has demonstrated that the ansatz

$$\text{Im} \Omega(s, b) = -\frac{\rho_0(s)}{2} \tilde{\sigma}(s, b) \quad (41)$$

gives a satisfactory description of the experimental data in the  $-t \leq 2.5 \text{ GeV}^2$  region, with a small coefficient of proportionality that was denoted in Ref. [33] by  $\alpha \propto \rho_0$  parameter. This ansatz assumes that the inelastic collisions at low four-momentum transfers correspond to the cases when the parts of proton suffer elastic scattering but these parts are scattered to different directions, not parallel to one another. This physical interpretation is actually due to  $\rho_0 \ll 1$  and  $\text{Im} \Omega(s, b) \ll 1$ . We will use this approximation below to demonstrate that the  $H(x)$  scaling function can have more complex shapes, that differ from  $H(x) = \exp(-x)$ .

Based on the results of the previous section obtained in the diffractive cone in the  $\rho_0 \ll 1$  and  $\tilde{\sigma}(s, b) \ll 1$  limit, we have the following scaling property of the opacity function:

$$\text{Re} \exp[-\Omega(s, b)] = 1 - r(s)E(\tilde{x}), \quad (42)$$

$$\text{Im} \exp[-\Omega(s, b)] = \rho_0(s) r(s)E(\tilde{x}), \quad (43)$$

$$\tilde{x} = b/R(s), \quad (44)$$

$$R(s) = \sqrt{B(s)}, \quad (45)$$

where  $r(s)$  is four times the ratio of the elastic to the total cross section, as given in Eq. (26), and  $E(\tilde{x})$  describes the distribution of the inelastic collisions as a function of the dimensionless impact parameter  $b$  normalised to  $\sqrt{B(s)}$ , the characteristic length-scale of the  $pp$  collisions at a given value of the center-of-mass energy  $\sqrt{s}$ .

This ansatz allows for a general shape of the impact parameter  $b$ -dependent scattering amplitude, that leads to a  $H(x)$  scaling. Under the assumption that the  $b$ -dependence may occur only through the two-dimensional scaling variable  $\tilde{x}$ , as described by the scaling function  $E(\tilde{x})$ ,

$$t_{\text{el}}(s, b) = (i + \rho_0(s)) r(s)E(\tilde{x}), \quad (46)$$

a general form of the  $H(x)$  scaling can be obtained. Here we assume that  $E(\tilde{x})$  is a real function that depends on the modulus of the dimensionless impact parameter  $\tilde{x} = b/R(s)$ . For normalization, we choose that the Fourier-transform  $\tilde{E}(0) = 1$ , which also corresponds to the condition

$$\int d^2 \tilde{x} E(\tilde{x}) = 1, \quad (47)$$

keeping in mind that we have two-dimensional Fourier-transform which at zero is equal to the integral over the two different directions in the impact-parameter space.

Let us investigate first the consequences of this scaling ansatz for the shadow profile function  $P(s, b)$ . The algebra



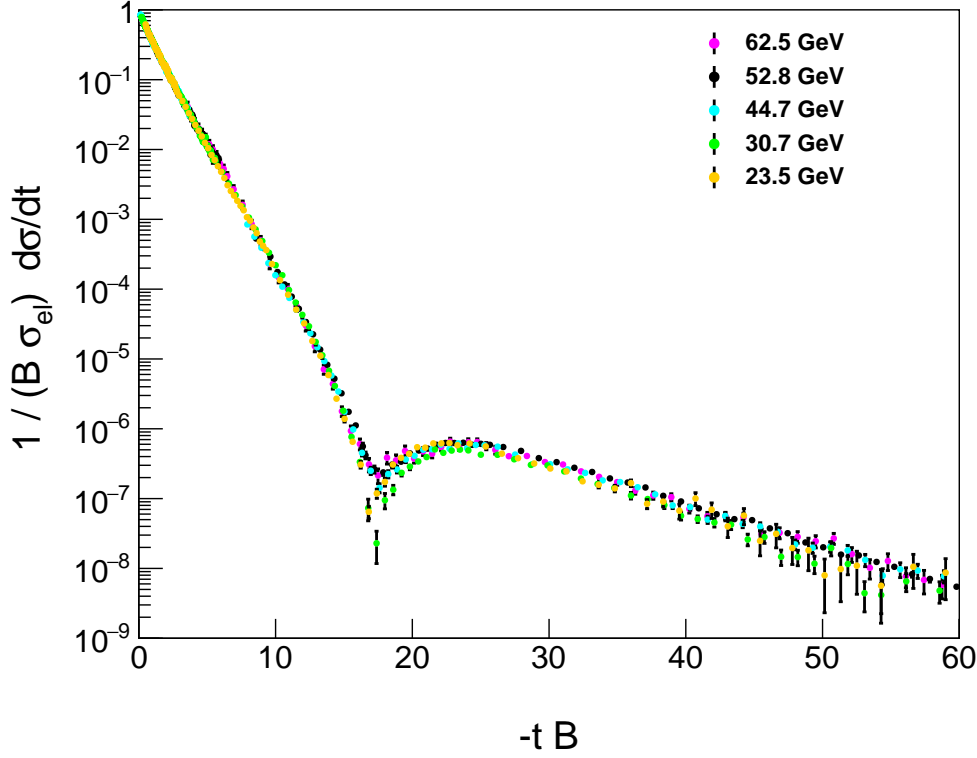


**Fig. 1** Scaling behaviour of the differential cross section  $d\sigma/dt$  of elastic  $pp$  collisions in the ISR energy range of  $\sqrt{s} = 23.5 - 62.5$  GeV. The measured differential cross section data are taken from Ref. [62] and references therein. These data are rescaled to  $H(x) = \frac{1}{B\sigma_{\text{el}}} \frac{d\sigma}{dt}$  as a function of  $x = -tB$ . This figure indicates a clear, better than expected data-collapsing behaviour.

is really very similar to that of the exponential cone approximation that was implemented above. We obtain the following result:

$$P(s, b) = \frac{1}{1 + \rho_0^2(s)} - (1 + \rho_0^2(s)) \left[ r(s) E\left(\frac{b}{R(s)}\right) - \frac{1}{1 + \rho_0^2(s)} \right]^2. \quad (48)$$

Evaluating the above relation at  $b = 0$  and using the normalization condition  $E(0) = 1$ , we obtain again that the shadow profile at zero impact parameter value has a maximum that is slightly less than unity:  $P(s, 0) \leq 1/(1 + \rho_0^2)$ . It is interesting to note that the maximum in the profile function is reached at the same threshold (28) as in the case of the exponential cone approximation, corresponding to

$$r(s)|_{\text{threshold}} = \frac{1}{1 + \rho_0^2(s)}, \quad (49)$$

$$\left. \frac{\sigma_{\text{el}}}{\sigma_{\text{tot}}} \right|_{\text{threshold}} = \frac{1}{4(1 + \rho_0^2(s))}. \quad (50)$$

Thus a threshold-crossing behaviour seems to happen if the elastic-to-total cross-section ratio exceeds 0.25. Remarkably, in the domain of validity of our derivation, this threshold

crossing point is independent of the detailed shape of the  $H(x)$  scaling function for a broad class of models. However, it is also clear from Eq. (48) that the shape of  $E(\tilde{x})$  function plays an important role in determining the hollowness effect, so a detailed precision shape analysis is necessary to obtain the significance of this effect.

Starting from the definition, Eq. (2), the scattering amplitude in the  $b$ -space (46) yields the following form of the differential cross section in the momentum space:

$$\frac{d\sigma}{dt} = \frac{1 + \rho_0^2(s)}{4\pi} r^2(s) R^4(s) |\tilde{E}(R(s)\Delta)|^2. \quad (51)$$

Utilizing Eq. (45), we find that this form of the differential cross section is dependent on the four-momentum transfer squared,  $t$ , indeed only through the variable  $x \equiv -B(s)t = R^2(s)\Delta^2$ , so it is a promising candidate to be a scaling variable.

Now, if we consider the function (51) at the optical point,  $t = 0$ , we find

$$A(s) = \left. \frac{d\sigma}{dt} \right|_{t=0} = \frac{1 + \rho_0^2(s)}{4\pi} r^2(s) R^4(s) |\tilde{E}(0)|^2. \quad (52)$$

If the impact parameter dependent elastic amplitude has an  $s$ -dependent internal scale and  $s$ -dependent strength, we thus obtain the following generalized scaling relation for arbitrary elastic scattering amplitudes that satisfy Eq. (46):

$$\frac{1}{A(s)} \frac{d\sigma}{dt} \equiv H(x) = \frac{|\tilde{E}(\sqrt{x})|^2}{|\tilde{E}(x=0)|^2}. \quad (53)$$

This scaling is derived for  $\rho_0 \ll 1$  and  $\tilde{\sigma}(s, b) \ll 1$ , and it indicates that the  $H(x)$  with a non-exponential scaling function is a very interesting theoretical possibility. Further generalizations of this derivation are possible and interesting but go clearly well beyond the scope of this manuscript, that aims to look for Odderon effects using the experimentally available information on this  $H(x)$  scaling and its possible violations.

In addition to providing an insight to the meaning of the non-exponential behaviour in the interference (dip and bump) region, the above derivation also clarifies meaning of the normalization of  $H(x)$ . In particular, the normalization of  $H(x)$  scaling function on the left hand side of Eq. (53) should be made by the value of the differential cross section at the optical ( $t = 0$ ) point as given by Eq. (52). This value for differential cross sections with nearly exponential diffractive cone is indeed approximately equal to  $A(s) = B(s)\sigma_{el}(s)$ . In this case, the normalization condition  $H(0) = 1$  is maintained, while the integral of  $H(x)$  becomes unity only for differential cross sections dominated by the exponential cone (i.e. when the integral contribution from the non-exponential tails is several orders of magnitude smaller as compared to the integral of the cone region).

For the total cross section, we find from Eq. (5)

$$\sigma_{tot}(s) = 2r(s)R^2(s)\tilde{E}(0) = \sqrt{\frac{16\pi A(s)}{1 + \rho_0^2(s)}}. \quad (54)$$

Note that here we have indicated the normalization just for clarity, but one should keep in mind that in our normalization,  $\tilde{E}(0) = 1$ , and correspondingly,  $H(x=0) = 1$  by definition.

As clarified by Eq. (53), the scaling function  $H(x)$  coincides with the modulus squared of the normalized Fourier-transform of the scaling function  $E(\tilde{x})$ , if the elastic amplitude depends on the impact parameter  $b$  only through its scale invariant combination  $x = \frac{b}{R(s)}$  and if  $\rho(s, t) \equiv \rho_0(s)$ . In this case, the  $H(x)$  scaling is directly connected to the impact parameter dependence of the elastic amplitude and transforms out the trivial  $s$ -dependencies coming from  $\sigma_{tot}(s)$ ,  $\sigma_{el}(s)$ ,  $B(s)$ , and  $\rho_0(s)$  functions. This approximation has enabled us to establish possible physical reasons of this new scaling, and to derive non-exponential shapes for the  $H(x)$  scaling function and to connect violations of the  $H(x)$  scaling to the hollowness effect in the shadow profile function of the proton at ultra-high energies. At the time of closing this

manuscript, the generalization of the above derivation to a  $t$ -dependent  $\rho(s, t)$  function is still incomplete, and will be the subject of a separate study. Nevertheless, in our numerical analysis of the  $H(x)$  scaling, detailed in the subsequent sections, in the comparisons of the scaled differential cross-sections and the deduced Odderon significance we have not imposed any  $\rho(s, t) \equiv \rho(s)$  condition, namely that the real to imaginary ratio is independent of  $t$  at any value of  $s$ , as the data analysis of our paper has been done on experimental data taken at their published value, without any theoretical assumptions. In this sense our main results, detailed in the subsequent sections are generic and do not rely on the assumption of a  $t$ -independent  $\rho(s, t)$ .

The above derivation also indicates that it is a promising possibility to evaluate the  $H(x)$  scaling function directly from the experimental data. It has a clear normalization condition,  $H(0) = 1$ . Furthermore, in the diffractive cone, for nearly exponential cone distributions,  $H(x) \approx \exp(-x)$ . We have shown in this section, that even if one neglects the possible  $t$  dependence of  $\rho(s, t)$ , arbitrary positive definite  $H(x)$  scaling functions can be introduced if the elastic amplitude is a product of  $s$ -dependent functions, and its impact parameter dependence originates only through an  $s$ -dependent scaling variable which can be conveniently defined as  $\tilde{x}^2 = \frac{b^2}{B(s)}$ . Thus, the violations of the  $H(x)$  scaling may happen if not only the slope parameter  $B(s)$ , the real-to-imaginary ratio  $\rho_0(s)$  and the integrated elastic and total cross sections  $\sigma_{el}(s)$  and  $\sigma_{tot}(s)$  depend on  $s$ , but also the  $b$ -dependence of the elastic scattering amplitude starts to change noticeably. Namely, the  $H(x)$  scaling breaks if the scaling relation  $t_{el}(b, s) = C(s)E(b/R(s))$  gets violated in the above mentioned case.

Finally, let us note that the leading order exponential shape of  $H(x) \approx \exp(-x)$  can be derived as a consequence of the analyticity of  $T_{el}(s, \Delta)$  at  $\Delta = 0$  corresponding to the  $t = 0$  optical point, as follows. By leading order we mean the result of a first order Taylor series expansion at  $x = 0$ , so in this leading order approximation,  $\exp(-x) \approx 1 - x$  up to second order effects. If  $T_{el}(s, \Delta)$  is an analytic function at  $\Delta = 0$ , then its leading order behaviour is  $T_{el}(s, 0) + c(s)\Delta$ , where  $c(s)$  is a complex coefficient that is in general dependent on  $s$ . Hence, the differential cross-section has the leading order behaviour  $d\sigma/dt \approx A(s)(1 + B(s)t + \dots)$  which up to leading order terms is the same as  $A(s)\exp(B(s)t)$ , which corresponds to the scaling function  $H(x) \approx \exp(-x)$ . Similar considerations, related to (non-)analyticity of modulus squared amplitudes and Lévy stable source distributions were introduced to Bose-Einstein correlations in high energy physics in ref. [65]. Although the functional behaviour of the  $H(x)$  function cannot be determined from analyticity beyond this leading order behaviour, its leading order term in  $x$  must thus be linear if the scattering amplitude is analytic at the optical  $t = 0$  point. On the other hand, our recent analysis

of the differential elastic cross sections in the LHC energy range [9, 26] suggests that this approximation breaks down since the TOTEM experiment observed a significant non-exponential behaviour already in the diffractive cone. In this case, at low values of  $|t|$ , nearly Lévy stable source distributions can be introduced, that lead to an approximate  $H(x) \propto \exp(-x^\alpha)$  behaviour, where  $\alpha = \alpha_{\text{Lévy}}/2 \leq 1$ . In this case, the leading order behaviour is non-analytic,  $H(x) \approx 1 - x^\alpha$ . We have shown in Refs. [9, 26], at low  $|t|$ , such a stretched exponential form with  $\alpha \simeq 0.9$  describes the elastic scattering data from ISR to LHC energies reasonably well in a very broad energy range from 23.5 GeV to 13 TeV.

## 5 Results in the TeV energy range

Keeping in mind that the  $H(x)$  scaling holds within experimental errors at the ISR energies, where the center-of-mass energies vary from 23.5 to 62.5 GeV, that is less than by a factor of three, let us also investigate the same scaling function at the LHC energies, where the TOTEM measurements span, on a logarithmic scale, a similar energy range, from 2.76 TeV to 13 TeV, i.e. slightly more than by a factor of four. The TOTEM data at 13, 7 and 2.76 TeV are collected from Refs. [1], [28], and Ref. [4], respectively, and plotted in Fig. 2. Note that the possible scaling violating terms are small in the  $\sqrt{s} = 2.76 - 7$  TeV region: they are within the statistical errors, when increasing  $\sqrt{s}$  from 2.76 to 7 TeV, i.e. by about a factor of 2.5. Let us also stress that we do not claim the validity of the  $H(x)$  scaling up to the top LHC energy of  $\sqrt{s} = 13$  TeV, as scaling violating terms start to be significant at that energy, in particularly close to the diffractive dip region.

Let us look into the scaling behaviour in the energy range of  $\sqrt{s} = 2.76 - 7$  TeV in more detail.

The left panel of Fig. 2 indicates that the  $H(x)$  scaling is valid within statistical errors in the  $\sqrt{s} = 2.76 - 7$  TeV energy range. The confidence level of this comparison corresponds to a CL = 99 % (statistical errors only). The right panel of the same Fig. 2 indicates that this scaling is violated, beyond systematic errors, if the  $\sqrt{s} = 13$  TeV data are also included to this comparison: the violation of the  $H(x)$  scaling by the 13 TeV data is focussed to the region of the diffractive dip. However, in the  $x < 10$  region, the  $H(x)$  scaling is approximately valid at each of these LHC energies of  $\sqrt{s} = 2.76, 7$  and 13 TeV. Instead of being approximately valid in the whole measurable  $x$  region, at the LHC this scaling remains valid at all these three LHC energies only through about 3-4 orders of magnitude drop in the differential cross-section at lower values of  $x$ . The so called “swing” effect becomes clear at  $\sqrt{s} = 13$  TeV: the scaling function starts to decrease faster than exponential before the diffractive minimum, and also the diffractive minimum moves to lower values in  $x$  as compared to its posi-

tion at lower LHC energies. This swing effect, apparent in Fig. 2, can be interpreted in terms of changes in the shadow profile of protons at the LHC energies as the energy range increases from 2.76 through 7 to 13 TeV. Indeed, such small  $s$ -dependent scaling violations in the  $H(x)$  scaling function show the same qualitative picture as what has been observed by the direct reconstruction of the  $P(s, b)$  shadow profiles in the TeV energy range in several earlier papers, see for example Refs. [37, 38, 66] or our Refs. [9, 26, 33].

Inspecting the left panel of Fig. 2, we find, that the  $H(x)$  scaling functions agree within statistical errors, if the colliding energy is increased from  $\sqrt{s} = 2.76$  TeV to 7 TeV. The right panel of the same figure shows that these data change significantly if the colliding energy increases further to  $\sqrt{s} = 13$  TeV. This implies that the possible scaling violating terms are small as they are within the statistical errors, when increasing  $\sqrt{s}$  from 2.76 to 7 TeV, by about a factor of 2.5. We have checked, that TOTEM preliminary data at  $\sqrt{s} = 8$  TeV also satisfy this  $H(x)$  scaling [67, 68].

However, this  $H(x)$  scaling is violated by  $s$ -dependent terms when increasing  $\sqrt{s}$  from 8 to 13 TeV, and such a scaling violation is significantly larger than the quadratically (maximally) added statistical and  $t$ -dependent systematic errors, as indicated on the right panel of Fig. 2.

This behaviour may happen due to approaching a new domain, where the shadow profile function of  $pp$  scattering changes from a nearly Gaussian form to a saturated shape, that in turn may develop hollowness at 13 TeV and higher energies. The experimental indications of such a threshold-crossing behaviour were summarized recently in Ref. [42], and are also described above: a new domain may be indicated by a sudden change of  $B(s)$  in between 2.76 and 7 TeV and, similarly, the crossing of the critical  $\sigma_{\text{el}}(s)/\sigma_{\text{tot}}(s) = 1/4$  line in multi-TeV range of energies, somewhere between 2.76 and 7 TeV. From the theoretical side, we have previously noted such a drastic change in the size of the proton substructure between the ISR and LHC energy domains from a dressed quark-like to a dressed di-quark type of a substructure [9, 26] which may be, in principle, connected to such a dramatic change in the scaling behaviour of the elastic cross section. However, in this work we focus on the scaling properties of the experimental data, and do not intend to draw any model-dependent conclusions.

Instead, on Fig. 3 we directly compare the  $H(x)$  scaling functions of the differential cross sections, using the same ISR and LHC data, as in Figs. 1 and 2, respectively. This range of data now spans nearly a factor of about 500, about a three orders of magnitude increase in the range of available colliding energies, from 23.5 GeV to 13 TeV. As can be seen in the corresponding Fig. 3, the scaling works approximately in the diffractive cone, however, the  $H(x)$  scaling function cannot be considered as an approximately constant if such a huge change in the colliding energies is considered.

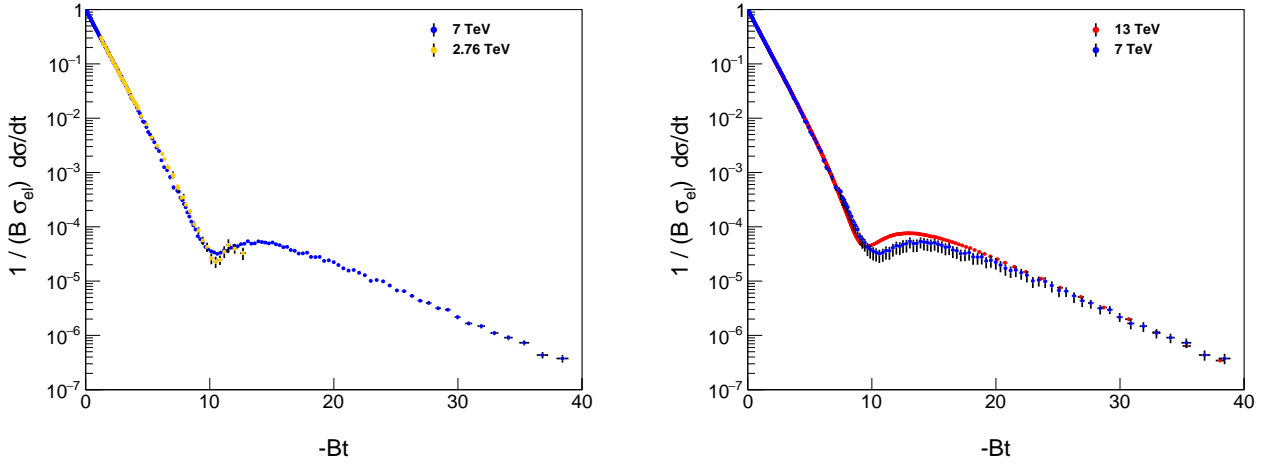


**Fig. 2** Scaling behaviour of the differential cross section  $d\sigma/dt$  of elastic  $pp$  collisions at LHC energies. Elastic scattering data are measured by the TOTEM Collaboration at  $\sqrt{s} = 13$  TeV [1], at  $\sqrt{s} = 7$  TeV [28], and at  $\sqrt{s} = 2.76$  TeV [4]. Left panel shows the 2.76 and 7 TeV data points with statistical errors only, while the right panel shows the 7.0 and 13.0 TeV data with statistical and  $t$ -dependent systematic errors added in quadrature. The left panel indicates, that the  $H(x)$  scaling is within statistical errors valid between  $\sqrt{s} = 2.76$  TeV and 7.0 TeV, so the  $H(x)$  scaling works from 7 TeV downwards. The right panel indicates that the  $H(x)$  scaling is violated, when the colliding energy is increased from  $\sqrt{s} = 7.0$  to 13 TeV: the right panel indicates scaling violations that go well beyond the combined statistical and systematic errors.

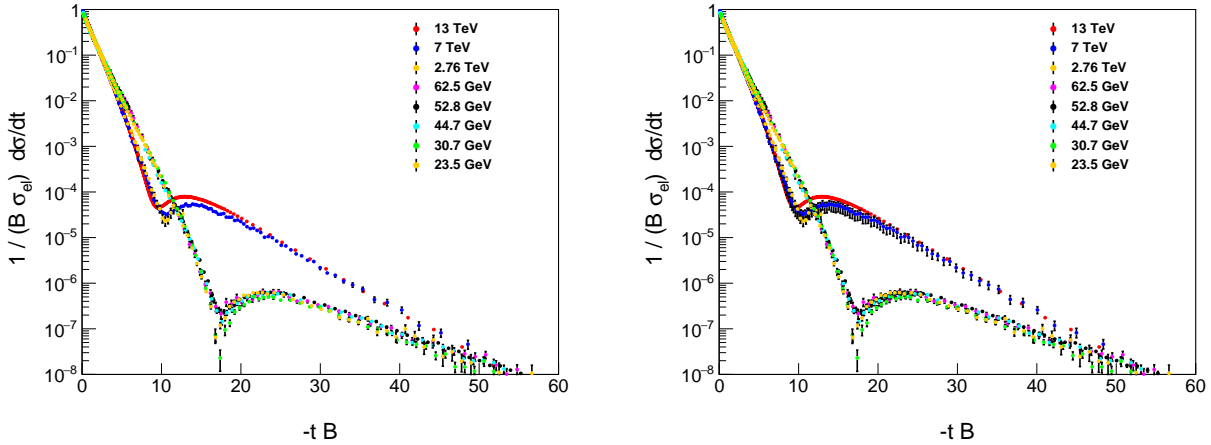


**Fig. 3** Scaling behaviour of the differential cross section  $d\sigma/dt$  of elastic  $pp$  collisions from ISR to LHC energies. Data points are the same as shown in Figs 1 and 2. (Left panel): Data points are shown with statistical errors only. (Right panel): Same data set, but now showing both statistical and  $t$ -dependent systematic errors added in quadrature.

Comparing Figs. 1, 2 and 3, we find that the  $s$ -dependence of the  $H(x)$  scaling functions is rather weak if  $s$  changes within a factor of two, however, there are very significant changes if the range of energies is changing by a factor of a few hundred, from the ISR energy range of  $\sqrt{s} = 23.5 - 62.5$  GeV to the LHC energy range of 2.76 – 7.0 – 13.0 TeV.

In the left panel of Fig. 4, the  $H(x)$  function of the  $\sqrt{s} = 2.76$  TeV TOTEM data set of Ref. [4] is compared with that of the  $p\bar{p}$  collisions measured by the D0 collaboration at  $\sqrt{s} = 1.96$  TeV Tevatron energy [8]. The right panel of Fig. 4 compares the  $H(x)$  scaling functions of elastic  $pp$  collision at  $\sqrt{s} = 7$  TeV LHC energy [28, 69] to that of the elastic  $p\bar{p}$

collisions at the Tevatron energy,  $\sqrt{s} = 1.96$  TeV. On both panels, the statistical errors and  $t$ -dependent systematic errors are added in quadrature. Lines are shown to guide the eye corresponding to fits with the model-independent Lévy series studied in Refs. [9, 26]. These plots suggest that the comparison of the  $H(x)$  scaling functions or elastic  $pp$  to  $p\bar{p}$  collisions in the TeV energy range is a promising method for the Odderon search, and a precise quantification of the difference between the  $H(x)$  scaling functions for  $pp$  to  $p\bar{p}$  collisions data sets is important. But how big is the difference between the  $H(x)$  scaling functions of elastic  $pp$  collisions at similar energies?



The  $H(x)$  scaling of the differential cross section  $d\sigma/dt$  of elastic  $pp$  collisions is compared at the nearby  $\sqrt{s} = 2.76$  and 7 TeV LHC energies on Fig. 5. These plots are similar to the panels of Fig. 4. The  $H(x)$  scaling functions are remarkably similar, in fact, they are the same within the statistical errors of these measurements. Due to their great similarity, it is important to quantify precisely how statistically significant their difference is.

We stress in particular that the possible scaling violations are small, apparently within the statistical errors, when  $pp$  results are compared at LHC energies and  $\sqrt{s}$  is increased from 2.76 to 7 TeV, by about a factor of 2.5. This makes it very interesting to compare the differential cross-sections of  $pp$  and  $p\bar{p}$  elastic scattering at the nearest measured energies in the TeV range, where crossing-odd components are associated with Odderon effects given that all Reggeon contributions are expected to be negligibly small in the TeV energy range. Actually, the largest  $\sqrt{s}$  of  $p\bar{p}$  elastic scattering data is 1.96 TeV, a measurement by the D0 collaboration [8] while at the LHC the public data set on the elastic  $pp$  scattering is available at  $\sqrt{s} = 2.76$  TeV [4], corresponding a change in  $\sqrt{s}$  by a factor of  $2.76/1.96 \approx 1.4$ . This is a rather small multiplicative factor on the logarithmic scale, relevant to describe changes both in high energy  $pp$  and  $p\bar{p}$  collisions. Given that the  $H(x)$  scaling function is nearly constant between 2.76 TeV and 7 TeV within the statistical errors of these data sets, we will search for a significant difference between the  $H(x)$  scaling function of elastic  $pp$  collisions at  $\sqrt{s} = 2.76$  and 7 TeV as well as that of the elastic  $p\bar{p}$  scattering at  $\sqrt{s} = 1.96$  TeV. If such a difference is observed, then there must be a crossing-odd (Odderon) component in the scattering amplitude of elastic  $pp$  and  $p\bar{p}$  scatterings.

Let us now consider Fig. 6. This plot compares the  $H(x)$  scaling functions for  $p\bar{p}$  collisions at various energies from  $\sqrt{s} = 546$  GeV to 1.96 TeV. Within experimental errors, an exponential cone is seen that extends to  $x = -tB \approx 10$  at each measured energies, while for larger values of  $x$  the scaling law breaks down in an energy dependent manner. At lower energies, the exponential region extends to larger values of  $x \approx 13$ , and the tail regions are apparently changing with varying colliding energies. Due to this reason, in this paper we do not scale the differential cross section of elastic  $p\bar{p}$  collisions to different values of  $\sqrt{s}$  as this cannot be done model-independently. This property of elastic  $p\bar{p}$  collisions is in contrast to that of the elastic  $pp$  collisions, where we have demonstrated in Figs. 1,2 that in a limited energy range between  $\sqrt{s} = 23.5$  and 62.5 GeV, as well as at the LHC in the energy range between  $\sqrt{s} = 2.76$  and 7 TeV, the  $H(x)$  scaling works well. Due to these experimental facts and the apparent violations of the  $H(x)$  scaling for  $p\bar{p}$  collisions in the  $x = -tB \geq 10$  region, in this paper we do not attempt to evaluate the energy dependence of the differential cross sections for  $p\bar{p}$  collisions. However, based on the

observed  $H(x)$  scaling in  $pp$  collisions, we do find a model-independent possibility to rescale the differential cross sections of elastic  $pp$  collisions in limited energy ranges.

After the above qualitative discussion of  $H(x)$  scaling for both  $pp$  and  $p\bar{p}$  elastic collisions, let us work out the details of the possibility of rescaling the measured differential cross sections to other energies in the domain where  $H(x)$  indicates a scaling behaviour within experimental errors.

The left panel of Fig. 7 indicates the result of rescaling of the differential cross sections of elastic  $pp$  scattering from the lowest  $\sqrt{s} = 23.5$  GeV to the highest 62.5 GeV ISR energy, using Eq. (66). We have evaluated the level of agreement of the rescaled 23.5 GeV  $pp$  data with the measured 62.5 GeV  $pp$  data with the help of Eq. (59). The result indicates that the data measured at  $\sqrt{s} = 25.5$  GeV and duly rescaled to 62.5 GeV are, within the errors of the measurements, consistent with the differential cross section of elastic  $pp$  collisions as measured at  $\sqrt{s} = 62.5$  GeV. This demonstrates that our method can also be used to extrapolate the differential cross sections at other energies by rescaling, provided that the  $H(x)$  scaling is not violated in that energy range and that the nuclear slope and the elastic cross sections are known at a new energy as well as at the energy from where such a rescaling starts.

A similar method is applied at the LHC energies in the middle panel of Fig. 7. This plot also indicates a clear agreement between the 2.76 TeV data and the rescaled 7 TeV data, which corresponds to a  $\chi^2/\text{NDF} = 39.3/63$  and a CL of 99.2 % and a deviation on the 0.01  $\sigma$  level only. This suggests that indeed the rescaling of the differential cross section of elastic scattering can be utilized not only in the few tens of GeV range but also in the few TeV energy range. Most importantly, this plot indicates that there is a scaling regime in elastic  $pp$  collisions, that includes the energies of  $\sqrt{s} = 2.76$  and 7 TeV at LHC, where the  $H(x)$  scaling is within errors, not violated. This is in a qualitative contrast to the elastic  $p\bar{p}$  collisions at TeV energies, where the validity of the  $H(x)$  scaling is limited only to the diffractive cone region with  $x \leq 10$ , while at larger values of  $x$ , the  $H(x)$  scaling is violated.

The right panel of Fig. 7 indicates a surprising agreement: after rescaling of the differential cross section of elastic  $pp$  collisions from 2.76 TeV to 1.96 TeV, we find no significant difference between the rescaled 2.76 TeV  $pp$  data with the  $p\bar{p}$  data at the same energy,  $\sqrt{s} = 1.96$  TeV. The agreement between the extrapolated  $pp$  and the measured  $p\bar{p}$  differential cross sections correspond to an agreement at a CL of 7.9 %, i.e. a surprising agreement at the 1.76 $\sigma$  level. It can be seen on the right panel of Fig. 7 that in the swing region, before the dip, the rescaled  $pp$  differential cross section seems to differ qualitatively with the  $p\bar{p}$  collisions data. However, according to our  $\chi^2$  analysis that also takes into account the horizontal errors of the TOTEM data, we find

that this apparent qualitative difference between these two data sets is quantitatively not significant: it is characterized as an agreement within less than  $2\sigma$ .

These plots suggest that the  $H(x)$  scaling functions of elastic  $pp$  and  $p\bar{p}$  collisions differ at similar energies, while the same scaling functions for elastic  $pp$  collisions are similar at similar energies, thus the comparison of the  $H(x)$  scaling functions of elastic  $pp$  and  $p\bar{p}$  collisions is a promising candidate for an Odderon search. Due to this reason, it is important to quantify how significant is this difference, given that the  $H(x)$  scaling functions scale out the dominant  $s$ -dependent terms, that arise from the energy-dependent  $\sigma_{el}(s)$  and  $B(s)$  functions. Such a quantification is the subject of the next section.

Before going into more details, we can already comment on a new Odderon effect qualitatively. When comparing the  $H(x)$  scaling function of the differential cross section of elastic  $pp$  collisions at 2.76 and 7.0 TeV colliding energies, we see no qualitative difference. By extrapolation, we expect that the  $H(x)$  scaling function may be approximately energy independent in a bit broader interval, that extends down to 1.96 TeV. Such a lack of energy evolution of the  $H(x)$  scaling function of the  $pp$  collisions is in a qualitative contrast with the evolution of the  $H(x)$  scaling functions of  $p\bar{p}$  collisions at energies of  $\sqrt{s} = 0.546 - 1.96$  TeV, where a qualitative and significant energy evolution is seen in the  $x = -tB > 10$  kinematic range. Thus, our aim is to quantify the Odderon effect in particular in this kinematic range of  $x = -tB > 10$  in order to evaluate the significance of this qualitative difference between elastic  $pp$  and  $p\bar{p}$  collisions.

## 6 Quantification

In this section, we investigate the question of how to compare the two different scaling functions  $H(x) = \frac{1}{B\sigma_{el}} \frac{d\sigma}{dt}$  with  $x = -tB$  introduced above measured at two distinct energies. We would like to determine if two different measurements correspond to significantly different scaling functions  $H(x)$ , or not. In what follows, we introduce and describe a model-independent, simple and robust method, that enables us to quantify the difference of datasets or  $H(x)$  measurements. The proposed method takes into account the fact that the two distinct measurements may have partially overlapping acceptance in  $x$  and their binning might be different, so the datasets may correspond to two different sets of  $x$  values.

Let us first consider two different datasets denoted as  $D_i$ , with  $i = 1, 2$ . In the considered case,  $D_i = \{x_i(j), H_i(j), e_i(j)\}$ ,  $j = 1, \dots, n_i$  consists of a set of data points located on the horizontal axis at  $n_i$  different values of  $x_i$ , ordered as  $x_i(1) < x_i(2) < \dots < x_i(n_i)$ ,  $H_i(j) \equiv H_i(x_i(j))$  are the measured values of  $H(x)$  at  $x = x_i(j)$  points, and  $e_i(j) \equiv e_i(x_i(j))$  is the corresponding error found at  $x_i(j)$  point.

In general, two different measurements have data points at different values of  $x$ . Let us denote as  $X_1 = \{x_1(1), \dots, x_1(n_1)\}$  the domain of  $D_1$ , and similarly  $X_2 = \{x_2(1), \dots, x_2(n_2)\}$  stands for the domain of  $D_2$ . Let us choose the dataset  $D_1$  which corresponds to  $x_1(1) < x_2(1)$ . In other words,  $D_1$  is the dataset that starts at a smaller value of the scaling variable  $x$  as compared to the second dataset  $D_2$ . If the first dataset ends before the second one starts, i.e. when  $x_1(n_1) < x_2(1)$ , their acceptances would not overlap. In the latter limiting case the two datasets cannot be compared using our method. Fortunately, however, the relevant cases e.g. the D0 data on elastic  $p\bar{p}$  collisions at  $\sqrt{s} = 1.96$  TeV have an overlapping acceptance in  $x$  with the elastic  $pp$  collisions of TOTEM at  $\sqrt{s} = 2.76, 7$  and 13 TeV. So from now on we consider the case with  $x_1(n_1) > x_2(1)$ .

If the last datapoint in  $D_2$  satisfies  $x_2(n_2) < x_1(n_1)$ , then  $D_2$  is within the acceptance of  $D_1$ . In this case, let us introduce  $f_2 = n_2$  as the final point with the largest value of  $x_f$  from  $D_2$ . If  $D_2$  has  $x_2(n_2) > x_1(n_1)$ , then the overlapping acceptance ends at the largest (final) value of index  $f_2$  such that  $x_2(f_2) < x_1(n_1) < x_2(f_2 + 1)$ . This means that the point  $f_2$  of  $D_2$  is below the largest value of  $x$  in  $D_1$ , but the next point in  $D_2$  is already above the final, largest value of  $x(n_1)$  in  $D_1$ .

The beginning of the overlapping acceptance can be found in a similar manner. Due to our choice of  $D_1$  as being a dataset that starts at a lower value,  $x_1(1) < x_2(1)$ , let us determine the initial point  $i_1$  in  $D_1$  that already belongs to the acceptance domain of  $D_2$ . This is imposed by the criterion that  $x_1(i_1 - 1) < x_2(1) < x_1(i_1)$ .

We compare the  $D_1$  and  $D_2$  datasets in the region of their overlapping acceptance, defined above, either in a one-way or in a two-way projection method. The projection  $1 \rightarrow 2$  has the number of degrees of freedom  $\text{NDF}(1 \rightarrow 2)$  equal to the number of points of  $D_2$  in the overlapping acceptance. For any of such a point  $x_i(2)$ , we used linear interpolation of the nearest points from  $D_1$  so that  $x_j(1) < x_i(2) \leq x_{j+1}(1)$  to evaluate the data and the errors of  $D_1$  at this particular value of  $x = x_i(2)$ . We used a linear interpolation using as a default (linear, exponential) scales in the  $(x, H(x))$  plane, that is expected to work well in the diffraction cone, where the exponential cone is a straight line. However, for safety and due to the unknown exact structure at the dip and bump region, we have also tested the linear interpolation utilizing the (linear, linear) scales in the  $(x, H(x))$  plane.

Similarly, the projection  $2 \rightarrow 1$  has the number of degrees of freedom  $\text{NDF}(2 \rightarrow 1)$  as the number of points of dataset  $D_1$  that fell into the overlapping common acceptance. A linear extrapolation was used for each  $x_i(1)$  points in this overlapping acceptance, so that  $x_j(2) < x_i(1) \leq x_{j+1}(2)$ , using both (linear, exponential) and (linear, linear) scales in the  $(x, H(x))$  planes.

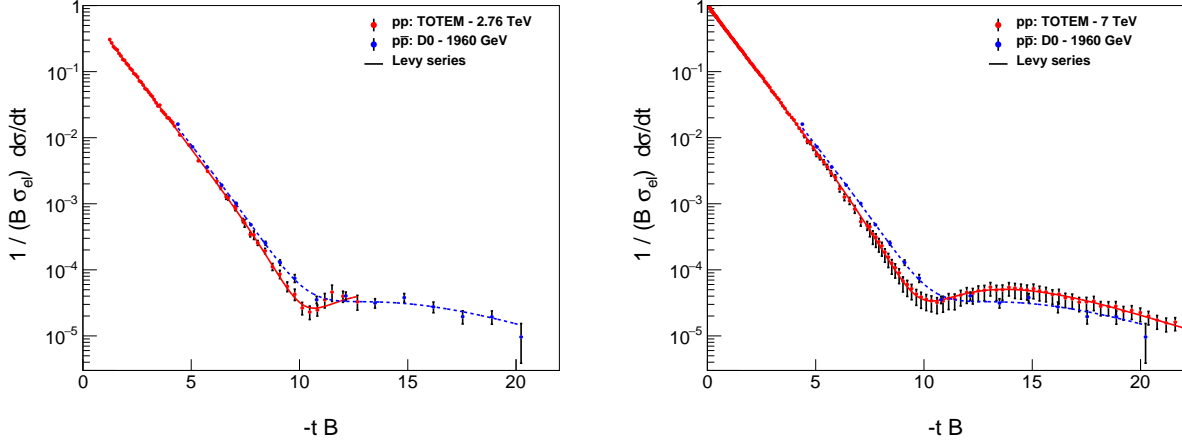


**Fig. 4** *Left panel:* Scaling function  $H(x) = \frac{1}{B\sigma_{\text{el}}} \frac{d\sigma}{dt}$  of the differential cross section of elastic  $pp$  collisions at  $\sqrt{s} = 2.76$  TeV LHC (red), as compared to that of the elastic  $p\bar{p}$  collisions at the Tevatron energy of  $\sqrt{s} = 1.96$  TeV (blue), shown as a function of  $x = -tB$ . *Right panel:* Same as the left panel, but now using elastic  $pp$  data at  $\sqrt{s} = 7$  TeV (red), as compared to elastic  $p\bar{p}$  collisions at  $\sqrt{s} = 1.96$  TeV (blue). On both panels, statistical errors and  $t$ -dependent systematic errors are added in quadrature. Lines are shown to guide the eye, corresponding to fits with the model-independent Lévy series from Refs. [9, 26].

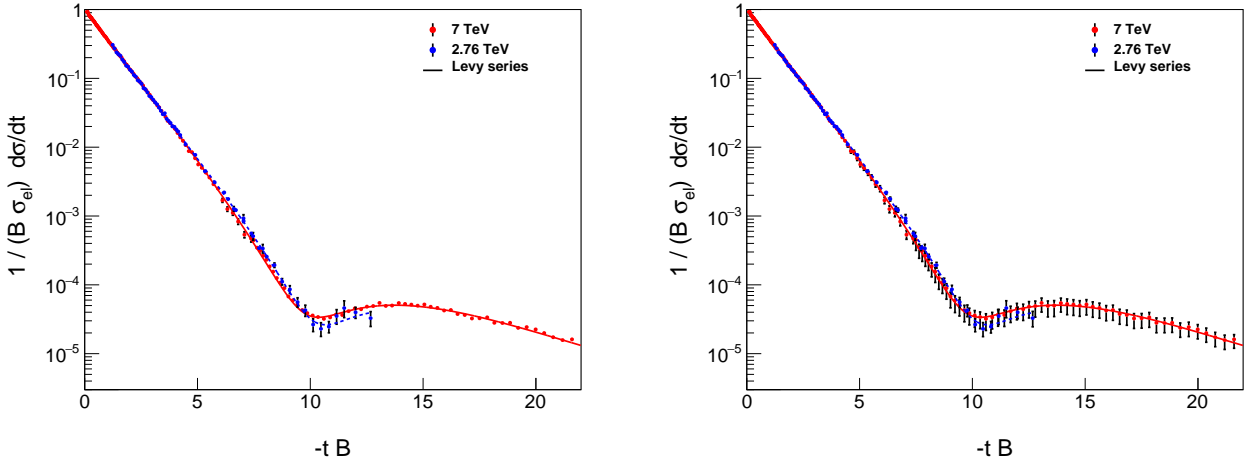


**Fig. 5** Same as Fig. 4, but now the  $H(x)$  scaling of the differential cross section  $d\sigma/dt$  of elastic  $pp$  collisions is compared at the nearby  $\sqrt{s} = 2.76$  and 7 TeV LHC energies. Left panel shows the data with statistical errors only, while on the right panel, statistical errors and  $t$ -dependent systematic errors are added in quadrature. The two  $H(x)$  scaling functions are, within statistical errors, apparently the same.

For the two-way projections, for example using  $1 \longleftrightarrow 2$  has the number of degrees of freedom is the sum of the points of  $D_1$  and  $D_2$  in the overlapping acceptance, defined as  $\text{NDF}(1 \longleftrightarrow 2) = \text{NDF}(1 \rightarrow 2) + \text{NDF}(2 \rightarrow 1)$

Let us describe the two-way projections in a bit more detail, as the one-way projections can be considered as special cases of this method.

A common domain  $X_{12} = \{x_{12}(1), \dots, x_{12}(n_{12})\}$  in the region of the overlap of the  $X_1$  and  $X_2$  domains can be introduced as follows.

Take the data points in the interval  $[i_1 \dots n_1]$  from the  $D_1$  set and the data points in the interval  $[1 \dots f_2]$  from the  $D_2$

set. This selection procedure provides a total of  $n_{12} = n_1 + f_2 - i_1 + 1$  points. Let us order this new set of points and denote such a united domain as  $X_{12}$ . This domain corresponds to a common acceptance region which has  $n_{12}$  data points on the horizontal axis denoted as  $\{x_{12}(1), \dots, x_{12}(n_{12})\}$ .

In order to compare the datasets  $D_1$  and  $D_2$ , one needs to build two analog datasets that are both extrapolated to the same common domain  $X_{12}$  starting from  $D_1$  and  $D_2$  as if the data in both analog datasets were measured at the same values of  $x$ . So far, either  $D_1$  or  $D_2$  has some data value on any element of the domain  $X_{12}$ , but only one of them is determined.

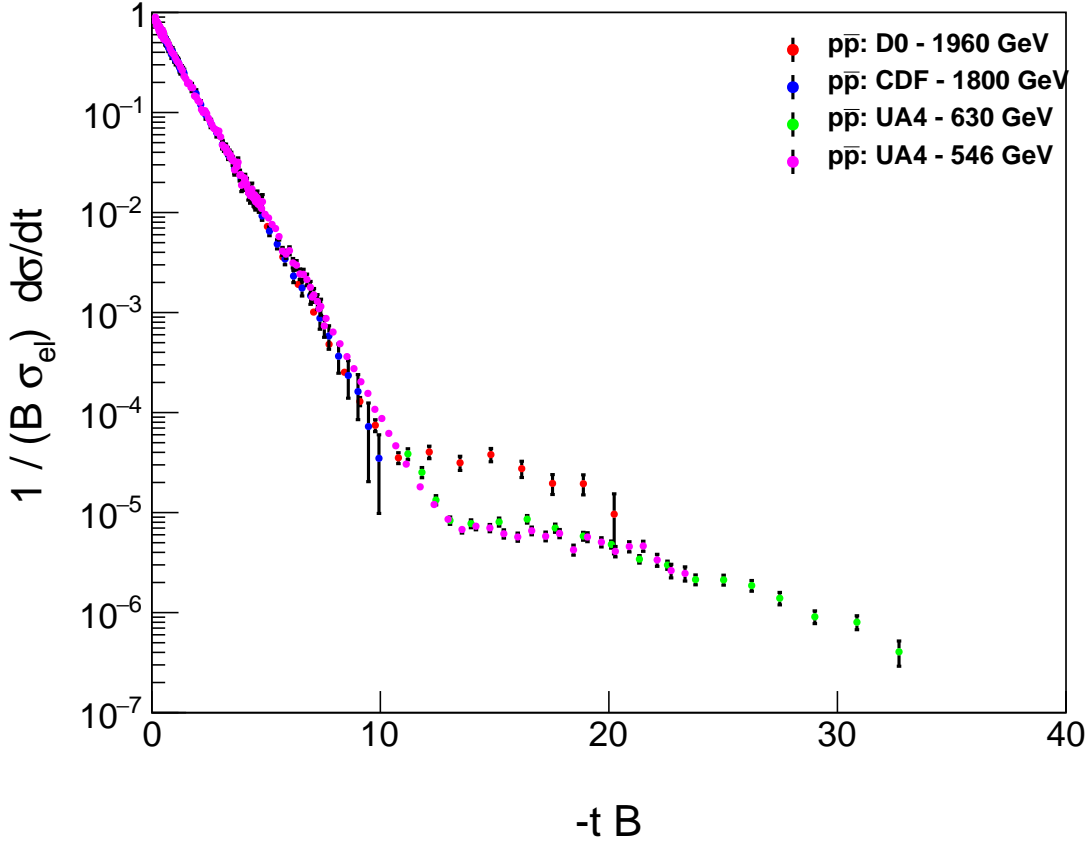


**Fig. 6** Approximate  $H(x) = \frac{1}{B\sigma_{\text{el}}} \frac{d\sigma}{dt}$  scaling of the differential cross section  $d\sigma/dt$  of elastic  $p\bar{p}$  collisions at  $\sqrt{s} = 0.546$  to  $1.96$  TeV. The scaling behaviour is valid in the exponential cone region, with the scaling function  $H(x) = \exp(-x)$ . The scaling domain starts at  $x = 0$  and extends up to  $x = -tB \simeq 10$ . Scaling violations are evident in the  $-tB \geq 10$  region, when the colliding energy increases from  $546$  GeV to  $1.96$  TeV, nearly by a factor of four.

Let us take first those points from  $X_{12}$  that belong to  $D_1$ , and label them with  $j$  index. There are  $n_1 - i_1 + 1$  such points. For such points, the data and error-bars of the extrapolated data set  $D_{12}$  will be taken from  $D_1$ :  $d_{12}(x_{12}(j)) = d_1(x_1(j))$ ,  $e_{12}(x_{12}(j)) = e_1(x_1(j))$ . However, for the same points,  $D_2$  has no measured value. But we need to compare the data of  $D_1$  and  $D_2$  at common values of  $x$ . So  $D_2$  data and errors can be interpolated using linear or more sophisticated interpolation methods. If the binning is fine enough, linear interpolation between the neighbouring datapoints can be used.

At this point, let us consider that in the diffractive cone, when an exponential approximation to the differential cross section can be validated, the shape of the scaling function is known to be  $H(x) \approx \exp(-x)$ . This function is linear on a (linear, logarithmic) plot of  $(x, H(x))$ . In what follows, we will test both a (linear, exponential) interpolation in the  $(x, H(x))$  plots (that is expected to give the best results in the diffractive cone) and a (linear, linear) interpolation that has

the least assumptions and that may work better than the (linear, exponential) interpolation technique around the diffractive minimum. These two different interpolation methods also allow us to estimate the systematic error that comes from the interpolation procedure itself. If the data points are measured densely enough in the  $(x, H(x))$  plot, both methods are expected to yield similar results. We present our final results using both techniques and note that indeed we find similar results with both methods.

Suppose that for the  $j$ -th point of data set  $D_{12}$  and for some  $i$  value of  $D_2$ ,  $x_2(i) < x_{12}(j) < x_2(i+1)$ . Then a linear interpolation between the  $i$ -th and  $i+1$ -th point of  $D_2$  yields the following formula:

$$d_{12}(j) = d_2(i) + (d_2(i+1) - d_2(i)) \frac{x_{12}(j) - x_2(i)}{x_2(i+1) - x_2(i)}. \quad (55)$$



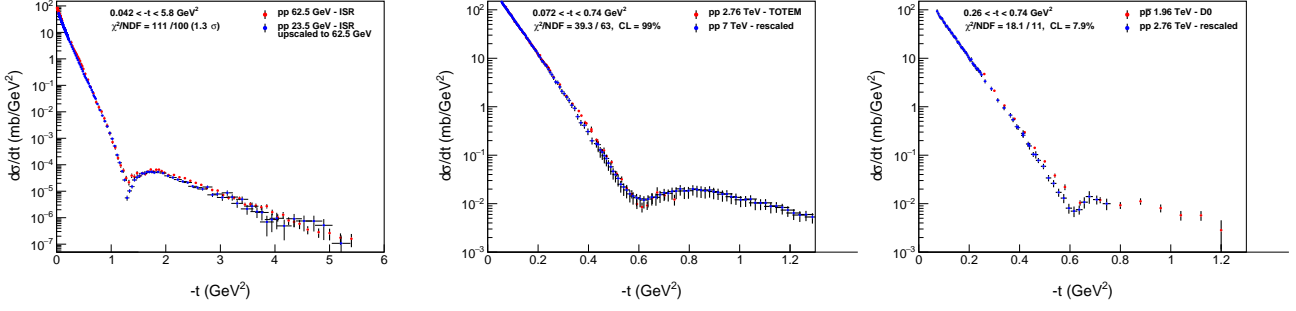


**Fig. 7** Rescaling of the differential cross section of elastic  $pp$  collisions at the ISR and LHC energies, using Eq. (66). This demonstrates that our method can also be used to get the differential cross sections at other energies by such a rescaling procedure, provided that the nuclear slope and the elastic cross sections are known at the new energy as well as at the energy from where we start to rescale the differential cross section. In both panels, we have evaluated the level of agreement between the rescaled and measured data with the help of Eq. (59). *Left panel:* Rescaling of the differential cross sections from the lowest ISR energy of  $\sqrt{s} = 23.5$  to the highest ISR energy of 62.5 GeV. The level of agreement between the rescaled 23.5 GeV  $pp$  data and the measured 62.5 GeV  $pp$  data corresponds to  $\chi^2/\text{NDF} = 111.0/110$  with a  $\text{CL} = 21.3\%$ , that indicates an agreement within  $1.3\sigma$ . *Middle panel:* Rescaling of the differential cross section of elastic  $pp$  collisions from the energy of  $\sqrt{s} = 7$  TeV [28, 69] down to 2.76 TeV [4]. *Right panel:* Rescaling of the differential cross section of elastic  $pp$  collisions from the energy of  $\sqrt{s} = 2.76$  TeV, measured by TOTEM [4], down to 1.96 TeV, where it is compared to the D0 dataset of Ref. [8]. The level of agreement between the rescaled 2.76 TeV  $pp$  data and the measured 1.96 TeV  $p\bar{p}$  data is quantified by a  $\chi^2/\text{NDF} = 18.1/11$  and a  $\text{CL} = 7.9\%$ , that indicates an agreement within  $1.8\sigma$ .

Similarly, the errors can also be determined by linear interpolation as

$$e_{12}(j) = e_2(i) + (e_2(i+1) - e_2(i)) \frac{x_{12}(j) - x_2(i)}{x_2(i+1) - x_2(i)}. \quad (56)$$

This way, one extends  $D_2$  to the domain  $X_{12}$ , corresponding to the overlapping acceptance of two measurements. If there is a measured value in  $D_2$ , we use that value and its error bar. If there is no measurement in  $D_2$  precisely at that given value of  $x$  that is part of the overlapping acceptance (corresponding to a value  $x$  from  $D_1$ ) then we use the two neighbouring points from  $D_2$  and use a (linear) interpolation to estimate the value at this intermediate point. This method works if the binning of both data sets is sufficiently fine so that non-linear structures are well resolved.

This way, for those  $j = 1, \dots, n_1 - i_1 + 1$  points from  $X_{12}$  that belonged to  $D_1$ , we have defined the data values from  $D_1$  by identity and defined the data points from  $D_2$  by linear interpolation from the neighbouring bins, so for these points both data sets are defined.

A similar procedure works for the remaining points in  $D_{12}$  that originate from  $D_2$ . There are  $f_2$  number of such points. Let us index them with  $k = 1, \dots, f_2$ . For these points, data and error-bars of the extrapolated data set  $D_{12}$  will be taken from  $D_2$ :  $d_{21}(x_{12}(k)) = d_2(x_2(k))$ , while the errors are given as  $e_{12}(x_{12}(k)) = e_2(x_2(k))$ . However, for the same points,  $D_1$  has no measured value. As we need to compare the data of  $D_1$  and  $D_2$  at common values of  $x$ , for these points,  $D_1$  data and errors can be extrapolated using the linear or more sophisticated interpolation methods based on the nearest measured points. If the binning is fine enough, linear interpolation between the neighbouring data-points

can be appropriately used. For broader bins, more sophisticated interpolation techniques may also be used that take into account non-linear interpolations based on more than two nearby bins, for example interpolations using Levy series expansion techniques of Ref. [9]. However, in the present manuscript such refinements are not necessary as the (linear, linear) and the (linear, exponential) interpolations in  $(x, H(x))$  give similar results.

Consider now that for the  $k$ -th point of data set  $D_{12}$  and for some  $l$ -th value of  $D_2$ ,  $x_1(l) < x_{12}(k) < x_1(l+1)$ . Then linear interpolation between the  $l$ -th and  $l+1$ -th point of  $D_2$  yields the following formula:

$$d_{21}(k) = d_1(l) + (d_1(l+1) - d_1(l)) \frac{x_{12}(k) - x_1(l)}{x_1(l+1) - x_1(l)}. \quad (57)$$

Similarly, the errors can also be determined by linear interpolation as

$$e_{21}(k) = e_1(l) + (e_1(l+1) - e_1(l)) \frac{x_{12}(k) - x_1(l)}{x_1(l+1) - x_1(l)}. \quad (58)$$

This way, using the linear interpolation techniques between the neighbouring data points, we can now compare the extended  $D_1$  and  $D_2$  to their common kinematic range:  $D_1$  was embedded and extrapolated to data points and errors denoted as  $d_{12}(x_{12})$  and  $e_{12}(x_{12})$  while  $D_2$  was embedded and extrapolated to data points and errors denoted as  $d_{21}(x_{12})$  and  $e_{21}(x_{12})$ , respectively. Note that the domain of both of these extended data sets is the same  $X_{12}$  domain. The index “12” indicates that  $D_1$  was extended to  $X_{12}$ , while index “21” indicates that  $D_2$  was extended to domain  $X_{12}$ .

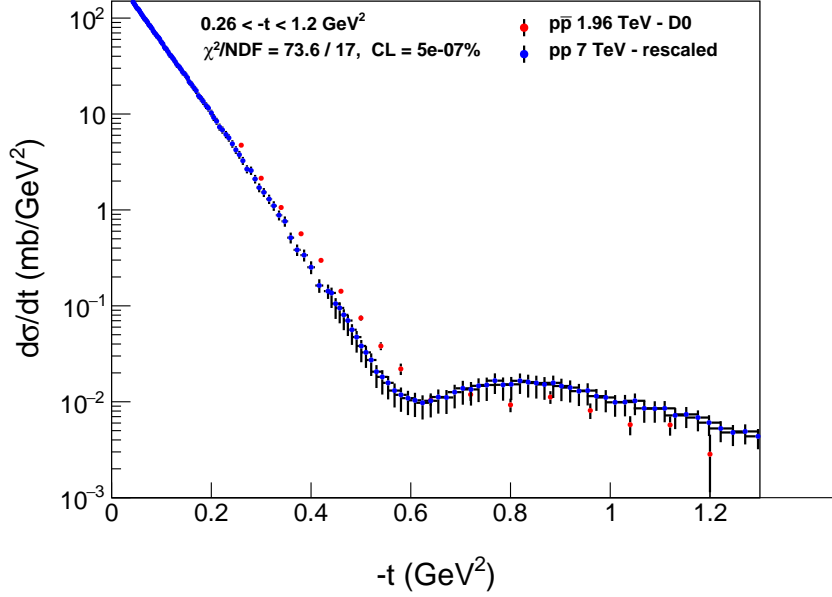


**Fig. 8** Rescaling of the differential cross section of elastic  $pp$  collisions from the energy of  $\sqrt{s} = 7$  to 1.96 TeV using Eq. (66). We have evaluated the confidence level of the comparison between the rescaled 7 TeV  $pp$  data set and the 1.96 TeV  $p\bar{p}$  data set with the help of Eq. (59), that does not take into account the horizontal errors of  $x$  coming from the slopes  $B$  and the type C point-to-point correlated errors on the vertical scale. Without these important effects, the difference between the datasets provides a  $\chi^2/NDF = 73.6/17$ , equivalent to a confidence level of  $CL = 5.13 \times 10^{-7}$  %, which corresponds to a difference at the  $5.84 \sigma$  level.

Now, we are done with the preparations to compare the two data sets, using the following  $\chi^2$  definition:

$$\chi^2 \equiv \chi_A^2 = \sum_{j=1}^{n_{12}} \frac{(d_{12}(j) - d_{21}(j))^2}{e_{12}^2(j) + e_{21}^2(j)}. \quad (59)$$

In this comparison, there are no free parameters, so the number of degrees of freedom is  $NDF = n_{12} = n_1 + f_2 - i_1 + 1$ , the number of data points in the unified data sample.

Based on the above Eq. (59) we get the value of  $\chi^2$  and NDF, which can be used to evaluate the  $p$ -value, or the confidence level (CL), of the hypothesis that the two data sets represent the same  $H(x)$  scaling function. If CL satisfies the criteria that  $CL > 0.1\%$ , the two data sets do not differ significantly. In the opposite case, if  $CL < 0.1\%$  the hypothesis that the two different measurements correspond to the same a priori  $H(x)$  scaling function, can be rejected.

The advantage of the above  $\chi^2$  definition by Eq. (59) is that it is straightforward to implement it, however, it has a drawback that it does not specify how to deal with the correlated  $t$  or  $x = -tB$  dependent errors, and horizontal or  $x$  errors. The  $t$  measurements at  $\sqrt{s} = 7$  TeV are published with their horizontal errors according to Table 5 of Ref. [28]. These errors should be combined with the published errors on the nuclear slope parameter  $B$  to get a horizontal error on  $x$  indicated as  $\delta x$ . Such a horizontal error has to be taken

into account in the final calculations of the significance of the Odderon observation.

Regarding the correlations among the measured values, and the measured errors, the best method would be to use the full covariance matrix of the measured differential cross section data. However, this covariance matrix is typically unknown or unpublished, with an exception of the  $\sqrt{s} = 13$  TeV elastic  $pp$  measurement by TOTEM [3]. Given that this TOTEM measurement of  $d\sigma/dt$  at 13 TeV indicates already the presence of small scaling violating terms in  $H(x)$  according to Fig. 2, this 13 TeV dataset cannot be used directly in our Odderon analysis, that is based on the  $s$ -independence of the scaling function of the differential elastic  $pp$  cross section  $H(x) \neq H(x, s)$  in a limited range that includes  $\sqrt{s} = 2.76$  and 7 TeV, but does not extend up to 13 TeV. However, we can utilize this TOTEM measurement of  $d\sigma/dt$  at 13 TeV, to test the method of diagonalization of the covariance matrix that we apply in our final analysis of the Odderon significance.

Our analysis of the covariance matrix relies on a method developed by the PHENIX Collaboration and described in detail in Appendix A of Ref. [70]. This method is based on the following separation of the various types of experimental uncertainties:

Type A) errors are point-to-point uncorrelated systematic uncertainties.

Type B) errors are point-to-point varying but correlated systematic uncertainties, for which the point-to-point correlation is 100 %, as the uncorrelated part is separated and added to type A) errors in quadrature.

Type C) systematic errors are point-independent, overall systematic uncertainties, that scale all the data points up and down by exactly the same, point-to-point independent factor.

Type D) errors are point-to-point varying statistical errors. These type D) errors are uncorrelated hence can be added to type A) errors in quadrature.

In this paper, where we apply this method to compare two different  $H(x)$  scaling functions, we also consider a fifth kind of error, type E) that corresponds to the theoretical uncertainty, which we identify with the error of the interpolation of one of the (projected) data sets to the  $x$  values that are compared at some (measured) values of  $x$  to a certain measured data point at a measured  $x$  value. This type E) error is identified with the value calculated from the linear interpolation, described above, as given for each A), B), C) and D) type of errors similarly by Eq. (58). Type D) errors are added in quadrature to type A) errors, and in what follows we index these errors with the index of the data point as well as with subscripts  $a$ ,  $b$  and  $c$ , respectively.

Using this notation, Eq. (A16) of Ref. [70] yields the following  $\chi^2$  definition, suitable for the projection of dataset  $D_2$  to  $D_1$ , or  $2 \rightarrow 1$ :

$$\tilde{\chi}^2(2 \rightarrow 1) = \sum_{j=1}^{f_1} \frac{(d_1(j) - d_{21}(j) + \varepsilon_{b,1}e_b(j) + \varepsilon_{c,1}d_1(j)e_c)^2}{\tilde{e}_{a,1}^2(j)} + \varepsilon_{b,1}^2 + \varepsilon_{c,1}^2, \quad (60)$$

where  $\tilde{e}_{a,12}(j)$  is the type A) uncertainty of the data point  $j$  of the united data set  $D_{12}$  scaled by a multiplicative factor such that the fractional uncertainty is unchanged under multiplication by a point-to-point varying factor:

$$\tilde{e}_{a,1}(j) = e_{a,1}(j) \left( \frac{d_1(j) + \varepsilon_{b,1}e_b(j) + \varepsilon_{c,1}d_1(j)e_c}{d_1(j)} \right). \quad (61)$$

In these sums, there are  $\text{NDF}_1 = f_1 - i_1 - 1$  number of data points in the overlapping acceptance from dataset  $D_1$ . A similar sum describes the one-way projection  $1 \rightarrow 2$ , but there are  $\text{NDF}_2 = f_2$  points in the common acceptance. For the two-way projections, not only the number of degrees of freedom add up,  $\text{NDF}_{12} = \text{NDF}_1 + \text{NDF}_2$ , but also the  $\chi^2$  values are added as  $\chi^2(1 \leftrightarrow 2) = \chi^2(1 \rightarrow 2) + \chi^2(2 \rightarrow 1)$ .

Let us note at this point, that  $H(x)$  is a scaling function that is proportional to the differential cross section normalized by the integrated cross section. In this ratio, the overall, type C) point-independent normalization errors multiply both the numerator and the denominator, hence these type C) errors cancel out in  $H(x)$ . Given that these type C) errors are typically rather large, for example, 14.4 % for the D0 measurement of Ref. [8], it is an important advantage in

the significance computation that we use a normalized scaling function  $H(x)$ . So in what follows, we set  $\varepsilon_{c,1} = 0$  and rewrite the equation for the  $\chi^2$  definition accordingly. This effect increases the significance of a  $H(x)$ -scaling test.

The price we have to pay for this advantage is that we have to take into account the horizontal errors on  $x$  in order to not overestimate the significance of our  $\chi^2$  test. In this step, we follow the propagation of the horizontal error to the  $\chi^2$  as utilized by the so-called effective variance method of the CERN data analysis programme ROOT. This yields the following  $\chi^2$  definition that we have utilized in our significance analysis for the case of symmetric errors in  $x$ :

$$\tilde{\chi}^2(2 \rightarrow 1) = \sum_{j=1}^{n_{12}} \frac{(d_1(j) - d_{21}(j) + \varepsilon_{b,1}e_b(j))^2}{\tilde{e}_{a,1}^2(j) + (\delta x_1(j)d'_1(j))^2} + \varepsilon_{b,1}^2, \quad (62)$$

where  $\delta x_{12}(j)$  is the (symmetric) error of  $x$  in the  $j$ -th data point of the data set  $D_1$ , and  $d'_1(j)^2$  is the numerically evaluated derivative of the extrapolated value of the projected data point obtained with the help of a linear interpolation using Eq. (57). Such definition is valid when the type B) errors are known and are symmetric for the data set  $D_1$  and the errors on  $x$  are also symmetric. When the data set  $D_1$  corresponds to the D0 measurement of elastic  $p\bar{p}$  collisions, Ref. [8], we have to take into account that D0 did not publish the separated statistical and  $|t|$ -dependent systematic errors, but decided to publish their values added in quadrature. So we use these errors as type A errors and with this method, we underestimate the significance of the results as we neglect the correlations among the errors of the data points in the D0 dataset. The TOTEM published the  $|t|$ -dependent statistical type D) errors and the  $|t|$ -dependent systematic errors both for the 2.76 TeV and 7 TeV measurements of the differential cross sections [4, 28, 69], with the note that the  $|t|$ -dependent systematic errors are almost fully correlated. In these works, TOTEM did not separate the point-to-point varying uncorrelated part of the  $|t|$ -dependent systematic errors. We thus estimate the type A) errors by the statistical errors of these TOTEM measurements, we then slightly underestimate them, hence overestimate the  $\chi^2$  and the difference between the compared data sets. Given that they are almost fully correlated, we estimate the type B) errors by the point-to-point varying almost fully correlated systematic errors published by the TOTEM. We have tested this scheme by evaluating the  $\chi^2$  from a full covariance matrix fit and from the PHENIX method of diagonalizing the covariance matrix at  $\sqrt{s} = 13$  TeV, using the Lévy expansion method of Ref. [9]. We find that the fit with the full covariance matrix results the same minimum within one standard deviation of the fit parameters, hence the same significance as the fit with the PHENIX method of Appendix A of Ref. [70].

We have thus validated the PHENIX method of Ref. [70] for the application of the analysis of differential cross section at  $\sqrt{s} = 13$  TeV, together with the effective variance

method of the ROOT package. This validation is important as the full covariance matrix of the  $\sqrt{s} = 2.76$  TeV and 7 TeV measurements by TOTEM is not published, but the PHENIX method appended with the ROOT method of effective variances can be used to effectively diagonalize the covariance matrix and to get similar results within the errors of the analysis. In Section 9, we employ the preliminary  $\chi^2$  definition of Eq. (62) to estimate the significance of the Odderon signal in comparison of the  $H(x)$  scaling functions for elastic  $pp$  and  $p\bar{p}$  collisions. Our final  $\chi^2$  definition and the corresponding final results are described in Appendix A.

## 7 Extrapolations

In this section, we discuss how to extrapolate the data points to energies where measurements are missing. As we have found, for example, in the ISR energy range of  $\sqrt{s} = 23.5 - 62.5$  GeV the  $H(x)$  scaling function is independent of  $\sqrt{s}$  within errors. We show how to extrapolate data points to unmeasured energies, under the condition that in a given energy range,  $H(x)$  is independent of the collision energy,  $H(x) \neq H(x, s)$ . In general, such a feature has to be established or cross-checked experimentally. This case is important, given that we have shown before, for example in Fig. 5, that  $H(x)$  for  $pp$  collisions stays energy-independent within errors between the LHC energies of  $2.76 \text{ TeV} \leq \sqrt{s} \leq 7 \text{ TeV}$ . Furthermore, we have already shown that for  $p\bar{p}$  collisions,  $H(x) = H(x, s)$  in the energy range of  $0.546 \leq \sqrt{s} \leq 1.96$  TeV, as indicated in Fig. 6.

Let us denote two different center-of-mass energies between which  $H(x) = \text{const}(\sqrt{s})$  within the experimental errors as  $\sqrt{s_1}$  and  $\sqrt{s_2}$ . Analogically, we denote various observables as  $B_i \equiv B(s_i)$ ,  $\sigma_i \equiv \sigma_{el,i} \equiv \sigma_{el}(s_i)$ ,  $x_i \equiv B_i t$ .

The energy independence of the  $H(x)$  scaling function formally can be written as

$$H_1(x_1) = H_2(x_2) = H(x) \quad \text{if} \quad x_1 = x_2. \quad (63)$$

This simple statement has tremendous experimental implications. The equality  $x_1 = x_2$  means that the scaling function is the same, if at center-of-mass energy  $\sqrt{s_1}$  it is measured at  $t_1$  and at energy  $\sqrt{s_2}$  it is measured at  $t_2$ , so that

$$t_1 B_1 = t_2 B_2 \quad \text{if} \quad x_1 = x_2. \quad (64)$$

The equality  $H_1(x_1) = H_2(x_2) = H(x)$  is expressed as

$$\frac{1}{B_1 \sigma_1} \frac{d\sigma}{dt} \bigg|_{t_1=x/B_1} = \frac{1}{B_2 \sigma_2} \frac{d\sigma}{dt} \bigg|_{t_2=x/B_2}. \quad (65)$$

Putting these equations together, this implies that the experimental data can be scaled to other energies in an energy

range where  $H(x)$  is found to be independent of  $\sqrt{s}$  as follows:

$$\frac{d\sigma}{dt} \bigg|_{t_1} = \frac{B_1 \sigma_1}{B_2 \sigma_2} \frac{d\sigma}{dt} \bigg|_{t_2=t_1 B_1/B_2}. \quad (66)$$

With the help of this equation, the data points on differential cross sections can be scaled to various different colliding energies, if in a certain energy region the  $H(x)$  scaling holds within the experimental errors. In other words, the differential cross section can be rescaled from  $\sqrt{s_1}$  to  $\sqrt{s_2}$  by rescaling the  $|t|$ -variable using the ratio of  $B_1/B_2 = B(s_1)/B(s_2)$ , and by multiplying the cross section with the ratio  $\frac{B_1 \sigma_1}{B_2 \sigma_2}$ .

## 8 Results

In this section, we present our results and close the energy gap, as much as possible without a direct measurement, between the TOTEM data on elastic  $pp$  collisions at  $\sqrt{s} = 2.76$  and 7.0 TeV and D0 data on elastic  $p\bar{p}$  collisions at  $\sqrt{s} = 1.96$  TeV. This section is based on the application of Eq. (66) in this energy range. After the rescaling procedure, the resulting data set at the new energy is compared with the measured data quantitatively with the help of Eq. (59).

We have used the rescaling equation, Eq. (66) first to test and to cross-check, if the rescaling of the  $\sqrt{s} = 23.5$  GeV ISR data to other ISR energies works, or not. The left panel of Fig. 7 indicates that such a rescaling of the differential cross sections from the lowest ISR energy of  $\sqrt{s} = 23.5$  to the highest ISR energy of 62.5 GeV actually works well. The level of agreement of the rescaled 23.5 GeV  $pp$  data with the measured 62.5 GeV  $pp$  data has been evaluated with the help of Eq. (59). We found an agreement with a  $\chi^2/\text{NDF} = 111/100$ , corresponding to a CL = 21.3 % and a difference is at the level of  $1.25\sigma$  only. This result demonstrates that our rescaling method can also be used to get the differential cross sections at other energies, provided that the nuclear slope and the elastic cross sections are known at the new energy as well as at the energy from where we start the rescaling procedure.

Subsequently, one can also rescale the TOTEM data at  $\sqrt{s} = 2.76$  or 7 TeV to 1.96 TeV, given that  $H(x)$  is (within errors) energy independent in the range of 2.76 – 7 TeV, corresponding to nearly a factor of 2.5 change in  $\sqrt{s}$ , while the change in  $\sqrt{s}$  from 1.96 to 2.76 TeV is only a factor of 1.4. The right panel of Fig. 7 indicates that rescaling the differential elastic  $pp$  cross section from  $\sqrt{s} = 2.76$  to 1.96 TeV also gives valuable results. We have evaluated the confidence level of the comparison of the rescaled 2.76 TeV  $pp$  data with the 1.96 TeV  $p\bar{p}$  data with the help of Eq. (59). As was already mentioned above, we have found a surprising agreement with a  $\chi^2/\text{NDF} = 18.1/11$ , corresponding to a CL = 7.93 %, and a difference at the level of  $1.75\sigma$  only.



Another important result is illustrated in Fig. 8. This comparison indicates a difference between the rescaled  $\sqrt{s} = 7$  TeV elastic  $pp$  differential cross-section [28, 69] to the  $\sqrt{s} = 1.96$  TeV energy and to the corresponding  $p\bar{p}$  data measured at  $\sqrt{s} = 1.96$  TeV [8]. To obtain a first estimate, this difference is quantified with the help of Eq. (59) yielding a CL of  $5.13 \cdot 10^{-7} \%$ . As this method adds the statistical and systematic errors in quadrature, it underestimates the actual significance of the difference between the two data sets. Although this estimate already provides a significant, greater than  $5\sigma$  effect for the Odderon observation, corresponding to a significant,  $5.84\sigma$  difference between the  $pp$  dataset and the 1.96 TeV  $p\bar{p}$  dataset, however, the evaluation of this significance does not yet take into account the rather large overall normalization error of 14.4 % that has been published by the D0 collaboration. The comparison of the differential cross-sections is sensitive to such type C errors, hence this effect has to be taken into account in the final significance analysis, or the significance has to be finalized using the  $H(x)$  scaling function, where the type C errors of the absolute normalization cancel.

It can be seen in Fig. 8 that in the swing region, before the dip, the rescaled  $pp$  differential cross section differ significantly from that of  $p\bar{p}$  collisions. Although the estimates of statistical significances given in this Section are based on a  $\chi^2$  test that includes the  $|t|$ -dependent statistical errors and the  $|t|$ -dependent systematic errors added in quadrature, the values of  $\chi^2/\text{NDF}$  and significances given above can still be only considered as estimates. Indeed, although the  $|t|$ -dependent systematic errors on these  $\sqrt{s} = 7$  TeV data are known to be almost fully correlated, the covariance matrix is not publicly available at the time of closing this manuscript from the TOTEM measurement at  $\sqrt{s} = 7$  TeV. It is clear that the  $\chi^2$  is expected to increase if the covariance matrix is taken into account, and this effect would increase the disagreement between the measured  $p\bar{p}$  and the extrapolated  $pp$  differential cross sections at  $\sqrt{s} = 1.96$  TeV. Note, the above estimate of significances does not yet take into account the overall correlated,  $|t|$ -independent vertical uncertainty in the differential cross section measurements. This uncertainty shifts all the data points up or down by a common,  $|t|$ -independent factor and may also decrease the significance of the difference between the measured  $p\bar{p}$  and the extrapolated  $pp$  cross sections at  $\sqrt{s} = 1.96$  TeV.

So this indicates that we have to consider the proposed rescaling method as conservatively as possible, that allows us to take into account the statistical and  $|t|$ -dependent correlated systematic errors, as well as the  $|t|$ -independent correlated systematic errors. Such an analysis is presented in the next section, where we quantify the differences between the scaling functions  $H(x)$  of elastic  $pp$  and  $p\bar{p}$  collisions using the fact that  $H(x)$  is free of  $|t|$ -independent normalization errors.

## 9 A significant Odderon signal

In this section, we introduce a  $6.55\sigma$  preliminary Odderon signal, while Appendix A summarizes our final Odderon signal of an at least  $6.26\sigma$ . Both results are obtained by comparing the  $H(x)$  scaling functions of  $pp$  and  $p\bar{p}$  collisions.

We have found a significant Odderon signal by comparing the  $H(x)$  scaling functions of the differential cross section of elastic  $pp$  collisions with  $\sqrt{s} = 7$  TeV to that of  $p\bar{p}$  collisions with  $\sqrt{s} = 1.96$  TeV, as indicated in Fig. 10. The comparison is made in both possible ways, by comparing the  $pp$  data to the  $p\bar{p}$  data, and vice versa. The difference between these two datasets corresponds to at least a  $\chi^2/\text{NDF} = 84.6/17$ , giving rise to a CL of  $5.8 \times 10^{-9} \%$  and to a preliminary,  $6.55\sigma$  significance, obtained with the help of Eq. (62). The overall,  $|t|$ -independent normalization error of 14.4 % on the D0 data set cancels from this  $H(x)$ , and does not propagate to our conclusions.

These results are obtained for the  $\sigma_{\text{el}} = 17.6 \pm 1.1$  mb value of the elastic  $p\bar{p}$  cross section at  $\sqrt{s} = 1.96$  TeV, and for the linear-exponential interpolation in  $(x, H(x))$ . Using this method of interpolation, the nearest points were connected with a linear-exponential line, that corresponds to a straight line on a linear-logarithmic plot in  $(x, H(x))$ . We have used the published values of the differential cross sections  $\frac{d\sigma}{dt}$ , that of the nuclear slope parameter  $B$  and the measured value of the elastic cross section  $\sigma_{\text{el}}$  for 7 TeV  $pp$  elastic collisions. For the elastic cross section of  $p\bar{p}$  collisions at  $\sqrt{s} = 1.96$  TeV, we have numerically integrated the differential cross section with an exponential approximation at very low- $|t|$  that provided us with  $\sigma_{\text{el}} = 20.2 \pm 1.4$  mb.

We have systematically checked the effect of variations in our interpolation method by switching from the (linear-exponential) in  $(x, H(x))$  interpolation to a linear-linear one and by changing the value of the elastic  $p\bar{p}$  collisions from the numerically integrated differential cross-section value of  $\sigma_{\text{el}} = 20.2 \pm 1.4$  mb, which is an unusually large value, but equals within the quoted 14.4 % systematic error to the  $\sigma_{\text{el}} = 17.6 \pm 1.1$  mb value, that corresponds to the trend published by the Particle Data Group, see the Fig. 51.6, bottom panel, yellow line of Ref. [71]. The input values of the nuclear slope parameter  $B$  and the elastic cross-section  $\sigma_{\text{el}}$  are summarized in Table 1.

As part of our systematic studies, we have also changed the direction of the projection. The results are summarized in Table 2. They indicate that the improved version of Fig. 8, shown as the top left panel of Fig. 10 and evaluated with the help of our improved  $\chi^2$  definition of Eq. (62) corresponds to a conservative case of Odderon observation based on the  $\sqrt{s} = 7$  TeV TOTEM and the  $\sqrt{s} = 1.96$  TeV D0 data sets. This panel indicates that the Odderon signal is observed in this comparison with a preliminary, at least a  $6.55\sigma$  significance, indicating the power of our method of Odderon ob-

Energy (GeV)	$\sigma_{el}$ (mb)	$B$ (GeV <sup>-2</sup> )	Reference
1960 ( $p\bar{p}$ )	$17.6 \pm 1.1$ $20.2 \pm 1.4$	$16.86 \pm 0.2$	Fig. 51.6 of Ref. [71] from low $-t$ fit to data [8]
2760 ( $pp$ )	$21.8 \pm 1.4$	$17.1 \pm 0.3$	[45] [4]
7000 ( $pp$ )	$25.43 \pm 1.02$	$19.89 \pm 0.272$	[46] [28]

**Table 1** Summary table of the elastic cross-sections  $\sigma_{el}$ , the nuclear slope parameters  $B$ , and their sources or references.

servation. In addition to this, our final result includes a symmetry requirement and a robustness test described in [Appendix A](#). These effects decreased the significance of our Odderon observation, from a preliminary,  $\geq 6.55 \sigma$  effect to a final and *statistically significant*,  $\geq 6.26 \sigma$  effect.

We have checked the robustness of this result for several possible variations of the  $\chi^2$  definition. The consideration that was most successful in decreasing this significance was related to the fact that unlike the original PHENIX method of ref. [70], that was worked out for a theory to data comparison, in this manuscript we compare data to data. So we have adapted the PHENIX method of ref. [70], from a situation where there was a theoretical function without errors compared to data with errors to a situation where we compare two datasets and both of these datasets have the same type of errors. This slightly decreased the significance of the Odderon signal, from the value of a preliminary, at least  $6.55 \sigma$  to the final value of  $6.26 \sigma$ , as detailed in [Appendix A](#) of this manuscript. Given that both significances of the preliminary  $6.55 \sigma$ , detailed in this section, and  $6.26 \sigma$ , detailed in [Appendix A](#) are clearly and safely above the  $5 \sigma$  discovery threshold, this robustness test did not change our conclusions.

The detailed figures, that show the  $\chi^2(\epsilon_b)$  functions for each of these cases are summarized in the left and right panels of Fig. 9 for the comparison of the 7 TeV TOTEM data set with the 1.96 TeV D0 data set. Each plot indicates a clear, nearly quadratic minimum. The values of  $\chi^2$  at the minima are summarized in Table 2, together with other characteristics of significance, like the confidence level and the significance in terms of standard variations. Similarly, the  $\chi^2(\epsilon_b)$  functions for the comparison of the 2.76 TeV TOTEM data set with the 1.96 TeV D0 data set are summarized in Fig. 11. The values of  $\chi^2$  at the minima are given in Table 3, together with other relevant characteristics.

As summarized in Fig. 10, a significant Odderon signal is found in the comparison of the  $H(x)$  scaling functions of the differential elastic  $pp$  (at  $\sqrt{s} = 7.0$  TeV) vs  $p\bar{p}$  ( $\sqrt{s} = 1.96$  TeV) cross sections. The horizontal error bars are indicated by a properly scaled horizontal line or — at the

data point. The statistical (type A, point-to-point fluctuating) errors are indicated by the size of the vertical error bars ( $|$ ), while shaded boxes indicate the size of the (asymmetric) type B (point-to-point varying, correlated) systematic errors. The overall normalization errors ( $|t|$ -independent, type C errors) cancel from the  $H(x)$  scaling functions since they multiply both the numerator and the denominator of  $H(x)$  in the same way. The correlation coefficient of the  $|t|$ -dependent systematic errors,  $\epsilon_b$ , is optimized to minimize the  $\chi^2$  based on Eq. (62), and the values indicated in Fig. 10 correspond to the minimum of the  $\chi^2(\epsilon_b)$ . These  $\chi^2$  values, as well as the numbers of degrees of freedom (NDFs) and the corresponding confidence levels (CLs) are indicated on both panels of Fig. 10, for both projections. The  $\chi^2(\epsilon_b)$  functions are summarized in Fig. 9. The 1.96 TeV  $\rightarrow$  7 TeV projection has a preliminary statistical significance of  $6.55 \sigma$  of an Odderon signal, corresponding to a  $\chi^2/\text{NDF} = 84.6/17$  and  $\text{CL} = 5.78 \times 10^{-9} \%$ . [Appendix A](#) presents the robustness test of this result, and summarizes the result of our tests of various possible modifications of our  $\chi^2$  definition. It turns out that the symmetry requirement discussed in [Appendix A](#) slightly reduces this significance from a  $6.55 \sigma$  level to a  $6.26 \sigma$  level, safely above the  $5.0 \sigma$  discovery threshold, corresponding to a  $\chi^2/\text{NDF} = 80.1/17$  and  $\text{CL} = 3.7 \times 10^{-8} \%$ . Thus the probability of Odderon observation in this analysis is at least  $P = 1 - \text{CL} = 0.99999999963$ .

Fig. 10 illustrates some of the results of our systematic studies in four different panels described as follows. The top-left panel of this figure uses a linear-exponential interpolation in the  $(x, H(x))$  plane and uses the value of  $17.6 \pm 1.1$  mb for the elastic  $p\bar{p}$  cross section at  $\sqrt{s} = 1.96$  TeV. This case gives the lowest ( $6.55 \sigma$ ) significance for the Odderon observation from among the possible cases that we have considered in Fig. 10. The top-right panel is similar but for a linear-linear interpolation in the  $(x, H(x))$ . The bottom-left panel is similar to the top-left panel, but now using  $20.2 \pm 1.4$  mb for the elastic  $p\bar{p}$  cross section at  $\sqrt{s} = 1.96$  TeV and also using a linear-exponential interpolation in  $(x, H(x))$ . The bottom-right panel is similar to the bottom-left panel, but using a linear-linear interpolation method.

The results of the scaling studies for a comparison of elastic  $pp$  collisions at  $\sqrt{s} = 2.76$  TeV, measured by the TOTEM experiment at the LHC [4] to that of  $p\bar{p}$  collisions at  $\sqrt{s} = 1.96$  TeV, measured by D0 at the Tevatron [8] are summarized in Fig. 12. The top-left panel uses  $\sigma_{el} = 17.6 \pm 1.7$  mb and a linear-exponential interpolation method in  $(x, H(x))$ . The top-right panel is the same as the top-left panel, but for a linear-linear interpolation in  $(x, H(x))$ . The bottom-left panel is nearly the same as the top-right panel, but for  $\sigma_{el} = 20.2 \pm 1.4$  mb. The bottom-right panel is the same as the bottom-left panel, but for a linear-linear interpolation in  $(x, H(x))$ . Neither of these comparisons shows a significant difference between the  $H(x)$  scaling function of elastic  $pp$

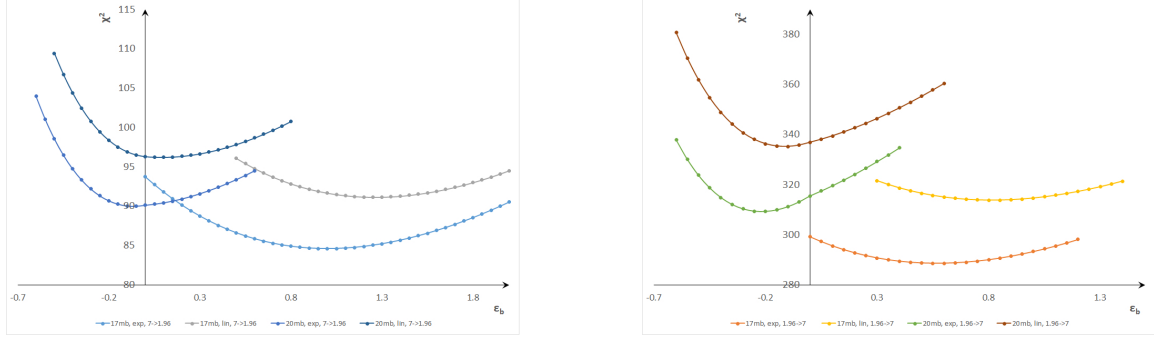


**Fig. 9** Dependence of  $\chi^2$  on the coefficient of the correlated but point-to-point varying systematic errors,  $\epsilon_b$ , for the comparison of the  $H(x)$  scaling functions of elastic  $p\bar{p}$  collisions at  $\sqrt{s} = 1.96$  TeV with that of  $pp$  collisions at  $\sqrt{s} = 7.0$  TeV. Each of the four cases are shown together corresponding to the direction of the projection. *Left panel* indicates the results of the  $1.96 \rightarrow 7.0$  TeV projection. *Right panel* indicates the results of the  $7.0 \rightarrow 1.96$  TeV projection. Both cases indicate four  $\chi^2(\epsilon_b)$  curves corresponding to the choice of linear-linear or linear-exponential interpolations in  $(x, H(x))$ , as well as to the choice of the elastic  $p\bar{p}$  cross section at  $\sqrt{s} = 1.96$  TeV ( $20.2 \pm 1.4$  mb vs  $17.6 \pm 1.1$  mb). A parabolic structure is seen in each case with a clear minimum, and the fit quality corresponding to these minima in  $\epsilon_b$  is summarized in Table 2.

$\sigma_{el}$ (mb)	interpolation	direction of comparison	$\chi^2$	NDF	CL [%]	Odderon significance in units of $\sigma$
$17.6 \pm 1.1$	lin-exp	7 --> 1.96 TeV	84.6	17	5.8E-09	6.55
		1.96 --> 7 TeV	289	65	5.3E-28	11.38
	lin-lin	7 --> 1.96 TeV	91.1	17	3.8E-10	6.94
		1.96 --> 7 TeV	314	65	2.6E-32	12.22
$20.2 \pm 1.4$	lin-exp	7 --> 1.96 TeV	90	17	6.1E-10	6.88
		1.96 --> 7 TeV	309	65	1.9E-31	12.05
	lin-lin	7 --> 1.96 TeV	96.2	17	4.5E-11	7.24
		1.96 --> 7 TeV	335	65	5.4E-36	12.89

**Table 2** Summary table of the significant Odderon signal in the one-way comparison of the  $H(x)$  scaling functions of  $pp$  collisions at  $\sqrt{s} = 7$  TeV measured by the TOTEM experiment at the LHC, and  $p\bar{p}$  elastic collisions at  $\sqrt{s} = 1.96$  TeV measured by the D0 experiment at Tevatron. This table indicates that the Odderon signal is observed in this comparison with at least a  $6.55\sigma$  significance. In [Appendix A](#) this is decreased to a significance of at least  $6.26\sigma$ . These significances are robustly above the  $5\sigma$  discovery threshold, corresponding to a statistically significant Odderon discovery.

collisions at  $\sqrt{s} = 2.76$  TeV as compared to that of  $p\bar{p}$  collisions at  $\sqrt{s} = 1.96$  TeV. It seems that the main reason for such a lack of significance is the acceptance limitation of the TOTEM dataset at  $\sqrt{s} = 2.76$  TeV, which extends up to  $x = -tB \approx 13$ , in contrast to the acceptance of the 7 TeV TOTEM measurement that extends up to  $x = -tB \approx 20$ . We have cross-checked this by limiting the 7 TeV data set also to the same acceptance region of  $4.4 < -Bt < 12.7$  as that of the 2.76 TeV data set. This artificial acceptance limitation has resulted in a profound loss of significance, down to  $\chi^2/\text{NDF} = 25.7/11$ , that corresponds to a CL = 0.71% and to a deviation at the  $2.69\sigma$  level only. This result indicates that if we limit the acceptance of the 7 TeV TOTEM measurement to the acceptance of the 2.76 TeV TOTEM

measurement, the significance of the Odderon observation decreases well below the  $5\sigma$  discovery threshold.

## 10 A summary of cross-checks

In this section, we summarize some of the most important cross-checks that we performed using our methods and results.

We have cross-checked what happens if one rescales the differential cross section of elastic  $pp$  scattering from the lowest ISR energy of  $\sqrt{s} = 23.5$  GeV to the top ISR energy of  $\sqrt{s} = 62.5$  GeV. As can be expected based on the approximate equality of all the  $H(x)$  scaling functions at the ISR energies, as indicated on the left panel of Fig. 7, the rescaled

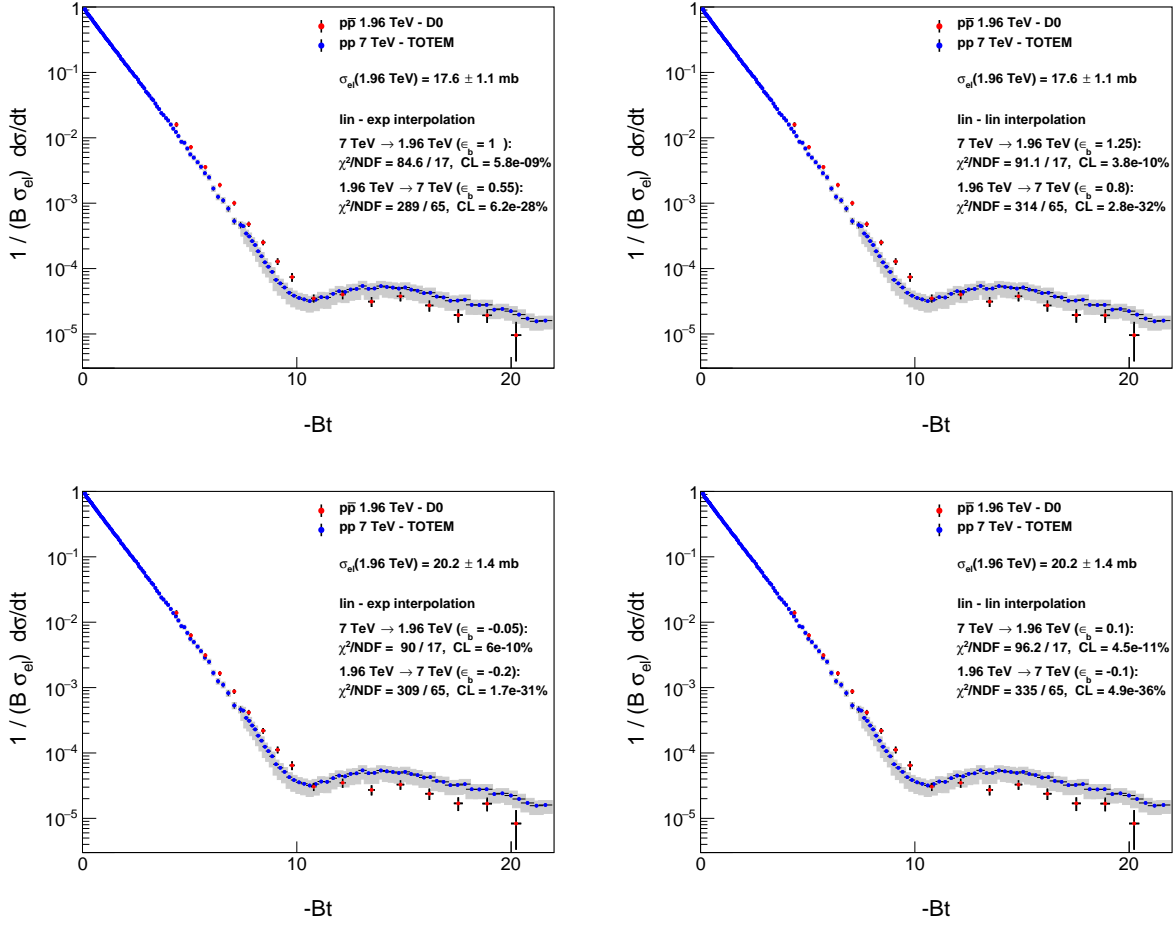


**Fig. 10** Odderon signal in the comparison of the  $H(x)$  scaling functions of  $pp$  collisions at  $\sqrt{s} = 7$  TeV, measured by the TOTEM experiment at the LHC [28, 69], and  $p\bar{p}$  elastic collisions at  $\sqrt{s} = 1.96$  TeV measured by the D0 experiment at Tevatron [8]. The results of this preliminary Odderon observation are summarized in Table 2, the final results are given in Appendix A. *Top-left panel*: This comparison uses  $17.6 \pm 1.1$  mb for the elastic  $p\bar{p}$  cross section at  $\sqrt{s} = 1.96$  TeV, and a linear-exponential interpolation technique in  $(x, H(x))$ . This corresponds to the smallest difference between the two data sets. *Top-right panel*: Same as the top-left panel but for linear-linear interpolations in the horizontal and vertical directions. For these interpolations, the nearest data points are connected with lines that correspond to a straight line on a linear-linear plot. *Bottom-left panel*: Same as the top-left panel but now using  $20.2 \pm 1.4$  mb for the elastic  $p\bar{p}$  cross section at  $\sqrt{s} = 1.96$  TeV. *Bottom-right panel*: Same as the bottom-left panel but using a linear-linear interpolation method.

23.5 GeV  $pp$  data coincide with the measured 62.5 GeV  $pp$  data. The resulting  $\chi^2/\text{NDF} = 111/100$  corresponds to a CL = 21.3 %, or a lack of significant difference – a  $1.3\sigma$  effect. In other words, our quantitative analysis indicates that the two data sets at the ISR energies of 23.5 and 62.5 GeV correspond to the same  $H(x)$  scaling function. This indicates that the method that we applied to extrapolate the 2.76 and 7 TeV data sets to lower energies satisfied the cross-checks at the ISR energies, i.e. our method works well. As one of the critical cross-checks of these calculations, two different co-authors coded the same formulae with two different codes using two different programming languages, and these codes were cross-checked against one another until both provided the same values of significances.

We have validated the PHENIX method of Ref. [70] implemented in the form of the  $\chi^2$  definition of Eq. (62) for the diagonalization of the covariance matrix on fits to the  $\sqrt{s} = 13$  TeV TOTEM data of ref. [3]. This PHENIX method resulted, within one standard deviation, the same minimum, hence the same significances, as the use of the full covariance matrix at  $\sqrt{s} = 13$  TeV elastic  $pp$  collisions. At the lower LHC energies of  $\sqrt{s} = 2.76$  and 7.0 TeV, due to the lack of publicly available information on the covariance matrix, only the PHENIX method of Ref. [70] was available for our final significance analysis.

We have also explored the main reason of the observation of a significant Odderon signal in the comparison of the  $H(x)$  scaling functions of elastic  $pp$  collisions at  $\sqrt{s} = 7$  TeV with that of the elastic  $p\bar{p}$  collisions at  $\sqrt{s} = 1.96$  TeV.



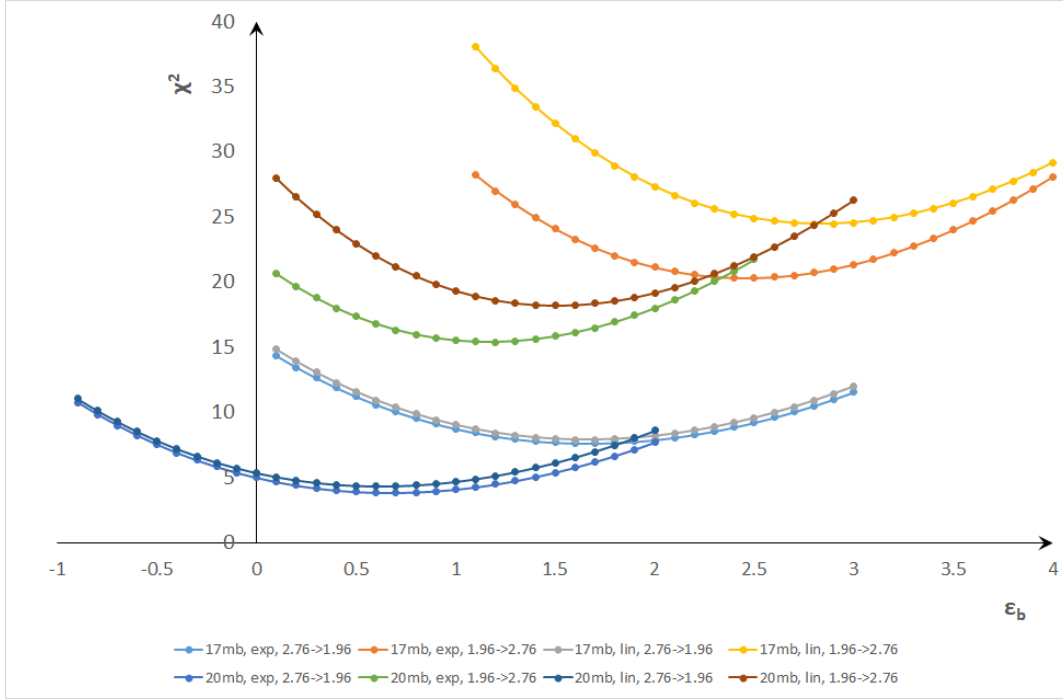


**Fig. 11** Dependence of  $\chi^2$  on the coefficient of the correlated but point-to-point varying systematic errors,  $\epsilon_b$ , for the comparison of the  $H(x)$  scaling functions of elastic  $p\bar{p}$  collisions at  $\sqrt{s} = 1.96$  TeV, measured by the D0 experiment at Tevatron [8], with that of elastic  $pp$  collisions at  $\sqrt{s} = 2.76$  TeV, measured by the TOTEM experiment at the LHC [4]. All the eight cases are shown together corresponding to the choice of linear-linear or linear-exponential interpolations in  $H(x)$ , to a different choice of the elastic cross section of  $p\bar{p}$  collisions at  $\sqrt{s} = 1.96$  TeV ( $20.2 \pm 1.4$  mb vs  $17.6 \pm 1.1$  mb), and to the direction of the projection ( $1.96 \rightarrow 2.76$  TeV, or  $2.76$  TeV  $\rightarrow 1.96$  TeV). A clear parabolic structure is seen in each case and the fit quality of the results that belong to these minima in  $\epsilon_b$  is summarized in Table 3.

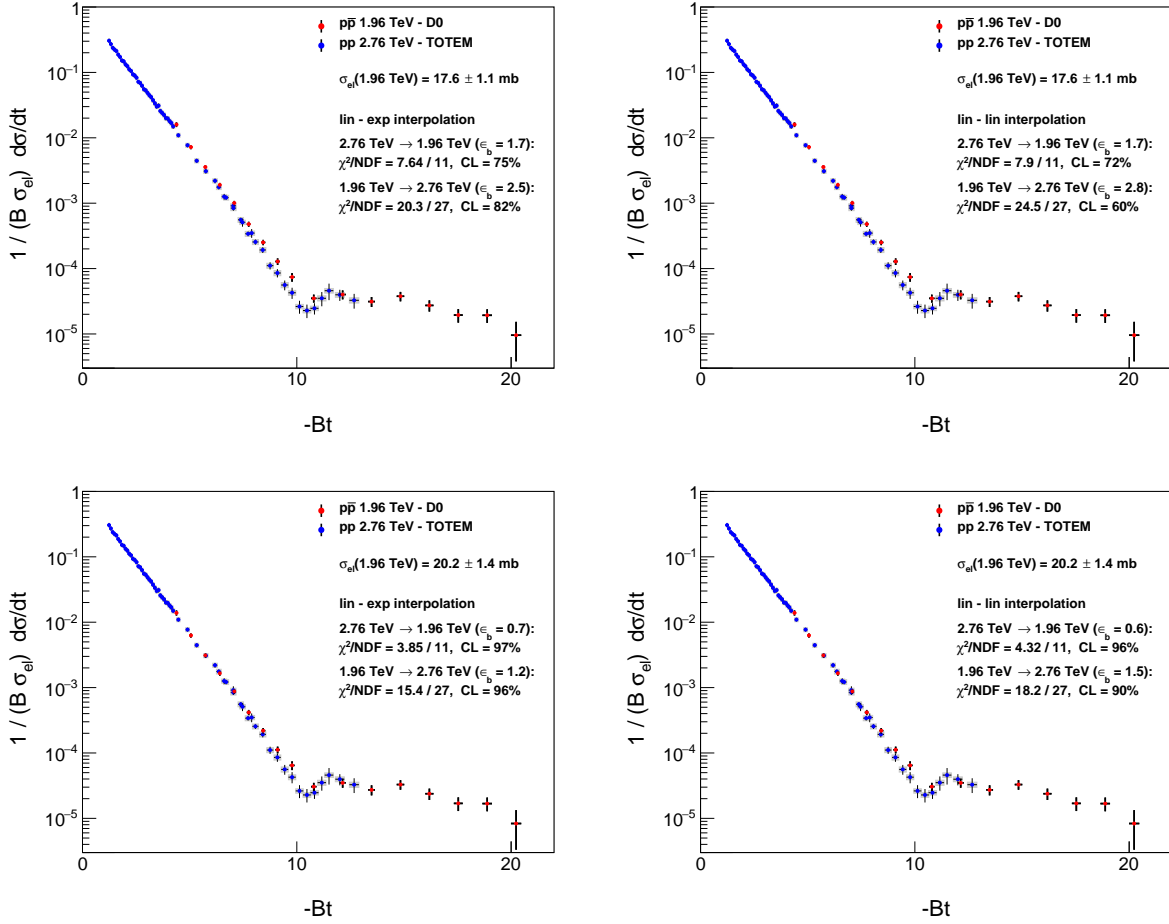
The question was rather intriguing as we have found no significant difference between the  $H(x)$  scaling functions of elastic  $pp$  collisions at  $\sqrt{s} = 2.76$  TeV and 7 TeV. At the same time, we also see that the comparison of the 2.76 TeV  $pp$  dataset to the 1.96 TeV  $p\bar{p}$  dataset does not indicate a significant Odderon effect. We have found that the Odderon signal vanishes from the comparison of the 7 TeV  $pp$  and the 1.96 TeV  $p\bar{p}$  datasets too, if we limit the acceptance of the 7 TeV dataset to the acceptance in  $x = -tB$  as that of the 2.76 TeV  $pp$  dataset: the significance of the Odderon observation decreased from an at least  $6.26\sigma$  discovery effect, detailed in Appendix A, to a  $2.69\sigma$  level agreement. We may note that a similar observation was made already in Ref. [10] that pointed out a strong  $|t|$  dependence of the Odderon contribution.

Table 4 summarises the search for an Odderon signal in the two-way comparison, for the significance of an Odderon signal in the comparison of the  $H(x)$  scaling functions of  $pp$  collisions at  $\sqrt{s} = 7$  TeV and  $p\bar{p}$  collisions at  $\sqrt{s} = 1.96$  TeV. Applying this method the Odderon signal is observed with at least a  $13\sigma$  significance, when both projections are

combined from Table 2, by adding the  $\chi^2$  and the NDF values of both directions of the comparisons.

## 11 Discussion

We have explored the scaling properties of the elastic differential cross sections at various energies, from the ISR up to the highest LHC energy. We have recalled that the earlier proposals for the  $F(y)$  and  $G(z)$  scaling functions were useful to explore if elastic scattering of protons in the LHC energy range is already close to the black-disc limit or not. After investigating several possible new dimensionless scaling variables and scaling function candidates, we have realized that in order to look for scaling violations in the low  $|t|$  kinematic range, corresponding to the diffractive cone it is advisable to scale all the diffractive cones to the same dimensionless scaling function,  $H(x) \approx \exp(-x)$ . This function can be obtained as the differential cross section normalized to its value at the optical point, which also for nearly exponential distributions equals to the elastic cross section  $\sigma_{el}$  multiplied by the slope parameter  $B$ . Both are readily measurable in elastic  $pp$  and  $p\bar{p}$  collisions, while other scaling



**Fig. 12** Lack of a significant Odderon signal in the comparison of the  $H(x)$  scaling functions of the differential cross section of elastic  $pp$  collisions with  $\sqrt{s} = 2.76$  TeV, measured by the TOTEM [4], to that of  $p\bar{p}$  collisions with  $\sqrt{s} = 1.96$  TeV, measured by D0 [8]. The correlation coefficient of the  $|t|$ -dependent systematic errors,  $\varepsilon_b$ , is optimized to minimize the  $\chi^2$  based on Eq. (62), and the value indicated on the plot corresponds to the minimum of  $\chi^2(\varepsilon_b)$ . The results of our Odderon search are summarized in Table 3. See also Table 5 for a summary of the results of the two-way comparisons of these  $H(x)$  scaling functions. *Top-left panel:* Using  $\sigma_{el} = 17.6 \pm 1.7$  mb and a linear-exponential interpolation method. *Top-right panel:* Same as the top-left panel but for a linear-linear interpolation in  $(x, H(x))$ . *Bottom-left panel:* Same as the top-left panel but for  $\sigma_{el} = 20.2 \pm 1.4$  mb. *Bottom-right panel:* Same as the bottom-left panel but for a linear-linear interpolation in  $(x, H(x))$ .

variables that we have investigated may depend on  $t_{dip}$  values – the location of the diffractive minimum, which however is not readily accessible neither in elastic  $p\bar{p}$  collisions (where there is no significant dip) nor in the acceptance limited elastic  $pp$  differential cross section (where the diffractive minimum may be located outside the acceptance of the experiment for that particular data set).

Given that the scaling function  $H(x)$  of elastic proton-(anti)proton scattering transforms out the energy dependence of the elastic slope  $B(s)$ , the real-to-imaginary ratio  $\rho_0(s)$  as well as the total and elastic cross sections,  $\sigma_{tot}(s)$  and  $\sigma_{el}(s)$ , Figs. 8 and 10 clearly indicate a crossing-odd component of the elastic scattering amplitude. At the  $\sim 2$  TeV energy scale, where the Reggeon contributions to the scattering amplitude are suppressed by their power-law decays, this is apparently a clear Odderon effect, a characteristic difference

in the shape of the scaling function of elastic scattering between  $pp$  and  $p\bar{p}$  collisions at the logarithmically similar energies of 7 and 1.96 TeV, respectively.

The effects due to the energy-induced difference between TOTEM and D0 data sets can be estimated by the lack of change of the  $H(x)$  scaling function for  $pp$  scattering between 2.76 TeV and 7 TeV, within the *statistical* errors of these TOTEM data sets. However, the  $H(x)$  scaling function of elastic  $pp$  scattering at  $\sqrt{s} = 7.0$  TeV is significantly different from the corresponding result of elastic  $p\bar{p}$  scattering at  $\sqrt{s} = 1.96$  TeV. These qualitative and quantitative differences, first, show up below the diffractive minimum of the  $pp$  elastic scattering, namely, the  $H(x)$  function for  $pp$  collisions indicates a strong “swing” or faster than exponential decrease effect, before developing a characteristic interference pattern consisting of a diffractive minimum and

$\sigma_{\text{el}}$ (mb)	interpolation	direction of comparison	$\chi^2$	NDF	CL [%]	Odderon significance in units of $\sigma$
$17.6 \pm 1.1$	lin-exp	2.76 --> 1.96 TeV	7.64	11	74.5	0.33
		1.96 --> 2.76 TeV	20.30	27	81.8	0.23
	lin-lin	2.76 --> 1.96 TeV	7.90	11	72.2	0.36
		1.96 --> 2.76 TeV	24.50	27	60.2	0.52
$20.2 \pm 1.4$	lin-exp	2.76 --> 1.96 TeV	3.85	11	97.4	0.03
		1.96 --> 2.76 TeV	15.40	27	96.3	0.05
	lin-lin	2.76 --> 1.96 TeV	4.32	11	96.0	0.05
		1.96 --> 2.76 TeV	18.20	27	89.7	0.13

**Table 3** Summary table of the search for an Odderon signal in the one-way comparison of the  $H(x)$  scaling functions of  $pp$  collisions at  $\sqrt{s} = 2.76$  TeV measured by the TOTEM experiment at the LHC, and  $p\bar{p}$  elastic collisions at  $\sqrt{s} = 1.96$  TeV measured by the D0 experiment at Tevatron.

$\sigma_{\text{el}}$ (mb)	interpolation	direction of comparison	$\chi^2$	NDF	CL [%]	Odderon significance in units of $\sigma$
$17.6 \pm 1.1$	lin-exp	7 <--> 1.96 TeV	373.6	82	8.3E-37	13.03
	lin-lin	7 <--> 1.96 TeV	405.1	82	3.0E-42	13.95
$20.2 \pm 1.4$	lin-exp	7 <--> 1.96 TeV	399	82	3.5E-41	13.78
	lin-lin	7 <--> 1.96 TeV	431.2	82	7.7E-47	14.69

**Table 4** Summary table of the search for an Odderon signal in the two-way comparison, for the significance of an Odderon signal in the comparison of the  $H(x)$  scaling functions of  $pp$  collisions at  $\sqrt{s} = 7$  TeV, measured by the TOTEM experiment at the LHC, and  $p\bar{p}$  elastic collisions at  $\sqrt{s} = 1.96$  TeV, measured by the D0 experiment at Tevatron. This table indicates that the Odderon signal is observed with at least a  $13\sigma$  significance, when both projections are combined from the previous Table 2, by adding the  $\chi^2$  and the NDF values of both directions of the comparisons. These results are remarkably stable with respect to the choice of the unknown integrated elastic cross section at  $\sqrt{s} = 1.96$  TeV, and also with respect to the choice of the linear-exponential or linear-linear interpolations. This effectively indicates that the combined significance of the Odderon discovery is at least a  $13\sigma$  effect.

subsequent maximum. In contrast, the D0 data on  $p\bar{p}$  elastic scattering features a structureless exponential decrease that in turn changes to a plateau or a shoulder-like structure at higher values of the scaling variable  $x$ . No clear indication of a diffractive maximum is seen in the  $p\bar{p}$  elastic scattering data [8], while the TOTEM data sets at each LHC energies of 2.76, 7 and 13 TeV clearly indicate a diffractive minimum followed by an increasing part of the differential cross section before the edge of the TOTEM acceptance is reached, respectively [3, 4, 69].

These qualitative and quantitative differences between the  $H(x)$  scaling functions of elastic  $pp$  and  $p\bar{p}$  scatterings provide a clear-cut and statistically significant evidence for a crossing-odd component in the scattering amplitude in the

TeV energy range. This corresponds to the observation of the Odderon exchange in the  $t$ -channel of the elastic scattering. The Odderon in this context is a trajectory that at  $J = 1$  contains a  $J^{\text{PC}} = 1^{--}$  vector glueball as well as other glueball states with higher angular momentum. Hence, one of the implication of our result is that not only one but several glueball states should exist in Nature.

Due to the presence of the faster-than exponentially decreasing (swing) region in elastic  $pp$  scatterings, the high-statistic  $pp$  elastic scattering data at  $\sqrt{s} = 1.96$  TeV may be taken as an additional measurement clearly closing the energy gap. However, the aperture limitation of the LHC accelerator is already resulting in a loss of significance of the comparison of the  $H(x)$  scaling function at 2.76 TeV with

$\sigma_{\text{el}}$ (mb)	interpolation	direction of comparison	$\chi^2$	NDF	CL [%]	Odderon significance in units of $\sigma$
$17.6 \pm 1.1$	lin-exp	2.76 <--> 1.96 TeV	27.9	38	88.4	0.15
	lin-lin	2.76 <--> 1.96 TeV	32.4	38	72.6	0.35
$20.2 \pm 1.4$	lin-exp	2.76 <--> 1.96 TeV	19.3	38	99.5	0.01
	lin-lin	2.76 <--> 1.96 TeV	22.5	38	97.8	0.03

**Table 5** Summary table of the search for an Odderon signal in the two-way comparison of the  $H(x)$  scaling functions of  $pp$  collisions at  $\sqrt{s} = 2.76$  TeV, measured by the TOTEM experiment at the LHC, and  $p\bar{p}$  elastic collisions at  $\sqrt{s} = 1.96$  TeV, measured by the D0 experiment at Tevatron. The lowest value of significance in this comparison is found to be  $0.01\sigma$ , which means that the  $H(x)$  scaling functions of 1.96 TeV  $p\bar{p}$  and 2.76 TeV  $pp$  elastic collisions are nearly the same within errors. The level of maximal difference is much less than a  $3\sigma$  effect which does not reach the statistical significance of a discovery effect in this comparison.

that of the D0 data at 1.96 TeV. Due to this reason, we propose an additional measurement of the dip and bump region of elastic  $pp$  collisions in the domain where the  $H(x)$  scaling was shown to work, in between 2.76 TeV and 7 TeV, if that can be harmonized with the LHC running schedule and scenarios.

The current TOTEM acceptance ends at  $-tB \approx 12$  at  $\sqrt{s} = 2.76$  TeV. Although more detailed acceptance studies are necessary, it seems that reaching  $x = -tB \approx 8 - 9$  seems to be a sufficient acceptance, as the swing effect in this range is already making a substantial and qualitative difference between the  $H(x) = (1/A)d\sigma/dt$  scaling functions of elastic  $pp$  and  $p\bar{p}$  collisions. New elastic  $pp$  scattering data around  $\sqrt{s} \approx 4 - 5$  TeV could be particularly useful to determine more precisely any possible residual dependence of these Odderon effects as a function of  $\sqrt{s}$ .

The current significance of the Odderon observation may be further increased from the  $6.26\sigma$  effect, but only by a tedious experimental re-analysis of some of the already published data, for example, by separating the point-to-point uncorrelated statistical and systematic errors (type A errors) from the point-to-point correlated systematic errors in elastic  $p\bar{p}$  collisions by D0, or, by the publication of the covariance matrix of the elastic cross section measurement of  $pp$  collisions at 2.76 and 7 TeV colliding energies by TOTEM. So taking more TOTEM data in special runs at new energies between  $\sqrt{s} = 2.76$  and 7.0 TeV seems to be a more enlightening and inspiring scenario, if it can be harmonized with LHC schedule and other ongoing experimental efforts.

## 12 Summary and conclusions

We have introduced a new, straightforwardly measurable scaling function  $H(x)$  of elastic proton-(anti)proton scattering. This scaling function transforms out the trivial energy-dependent factors, in particular, the effects due to the  $s$ -dependencies stemming from the elastic slope  $B(s)$ , from the real-to-imaginary ratio  $\rho_0(s)$ , as well as from the total and elastic cross sections,  $\sigma_{\text{tot}}(s)$  and  $\sigma_{\text{el}}(s)$ , respectively. In our numerical analysis of published data, the  $H(x)$  scaling and the deduced Odderon significance is obtained without theoretical assumptions. However, the established energy independence of the  $H(x)$  scaling as a property of the data in the few TeV energy range provides a strong constrain on model-building. Several simple models, like the simple eikonal amplitude of one-Pomeron-exchange lead to the violation of such a  $H(x)$  scaling. It follows that in the few TeV energy range, where the  $H(x)$  scaling is found to be valid, one-Pomeron exchange cannot be the only contribution to the scattering amplitude.

Figs. 8 and 10 clearly illustrate a qualitative and a quantitative difference between the scaling properties of the elastic  $pp$  and  $p\bar{p}$  collisions, corresponding to a crossing-odd component of the elastic scattering amplitude at the TeV energy scale. As in this kinematic region the Reggeon contributions to the scattering amplitude are suppressed by their power-law decays, a significant characteristic difference between the  $H(x)$  scaling functions of elastic  $pp$  and  $p\bar{p}$  collisions at the logarithmically similar energies of 7, 2.76 and 1.96 TeV is a clear-cut Odderon effect, because the trivial energy dependences of  $\sigma_{\text{el}}(s)$  and  $B(s)$  as well as that of  $\rho(s)$  and  $\sigma_{\text{tot}}(s)$  are scaled out from  $H(x)$  by definition.

A comparison in Fig. 10 indicates a significant difference between the rescaled 7 TeV  $pp$  data set down to 1.96

TeV with the corresponding  $p\bar{p}$  data measured at  $\sqrt{s} = 1.96$  TeV. Thus the re-analyzed D0 and TOTEM data, taken together with the verified energy independence of the  $H(x)$  scaling function in the  $\sqrt{s} = 2.76 - 7.0$  TeV energy range amount to the closing of the energy gap between 2.76 and 1.96 TeV in a model-independent way, as much as reasonably possible without a direct measurement.

At the same time, Fig. 5 indicates that the same 7 TeV data rescaled down to  $\sqrt{s} = 2.76$  TeV do not significantly differ from the TOTEM data measured at the same energy of 2.76 TeV, which is logarithmically close to 1.96 TeV, the highest available colliding energy of  $p\bar{p}$  elastic collisions. So, we have utilized the observed energy independence of the  $H(x)$  scaling function of elastic  $pp$  collisions in the few TeV energy range. One of the new, qualitative Odderon effects that we have identified was the approximate energy independence of the  $H(x)$  scaling function for elastic  $pp$  collisions in the few TeV energy range, in contrast to a stronger energy dependence of the  $H(x)$  scaling function for elastic  $p\bar{p}$  collisions.

Our final significance analysis is presented in Appendix A, resulting in an at least  $6.26\sigma$ , discovery level Odderon effect, corresponding to a  $\chi^2/\text{NDF} = 80.1/17$  and  $\text{CL} = 3.7 \times 10^{-8} \%$ . The probability of our Odderon observation is at least  $P = 1 - \text{CL} = 0.9999999963$ . Our analysis indicates that the statistically significant contribution to this Odderon signal is coming from the kinematic range of  $10 \leq x = -tB \leq 20$ . It is thus important to measure elastic scattering cross-sections at LHC at large  $-t$ , well beyond the diffractive cone. Elastic  $pp$  scattering data in a vicinity of  $\sqrt{s} \approx 2$  TeV as well as in between 2.76 and 7 TeV would be most useful for further detailing the Odderon properties.

In conclusion, we find from a model-independent re-analysis of the scaling properties of the differential cross sections of already published D0 and TOTEM data sets a statistically significant, more than a  $6.26\sigma$ , robust effect of  $t$ -channel Odderon exchange. Whatever we tried the significance of the Odderon observation remained safely above the  $5\sigma$  discovery threshold, with the most conservative significance estimate detailed in Appendix A.

## Appendix A: Cross-checking the $\chi^2$ definition: symmetric treatment

This Appendix summarizes our final, conservative and robust estimate of the significance of the Odderon observation in the compared D0 [8] and TOTEM [4, 28, 69] datasets, at  $\sqrt{s} = 1.96$  TeV for  $p\bar{p}$  and at  $\sqrt{s} = 2.76$  and 7 TeV for  $pp$  elastic scattering. Here we compare the considered data sets in a symmetric manner, and also mention some of the several robustness and quality tests that we have performed.

As a cross-check and a robustness test, we have validated the method with the help of a Levy-fit of ref. [9], confirming

that both methods (the fit with the full covariance matrix and the method described below) gave within one standard deviations the same minima with MINOS errors, error matrix accurate, fit in converged status and a statistically acceptable confidence level of  $\text{CL} \geq 0.1 \%$ . As a robustness test, the same analysis was repeated by two different co-authors of this manuscript using two different programming codes written in two different programming languages, providing the same results. In order to test the robustness of the results, have tried different possible definitions of  $\chi^2$  and the values reported in this Appendix correspond to the lowest possible significances.

Our final quantification of the Odderon significance is based on a method developed by the PHENIX collaboration in Ref. [70] using a specific  $\chi^2$  definition that effectively diagonalizes the covariance matrix. We utilized the measured differential cross-section of elastic  $pp$  scattering and its published covariance matrix at  $\sqrt{s} = 13$  TeV, as measured by TOTEM in ref. [3], for a validation of this method. We have adopted the PHENIX method of the diagonalization of the covariance matrix using type A, B and C errors [70].

In its original form, the experimental data that have statistical and systematic errors are compared to a theoretical calculation that is assumed to be a function of the fit parameters. In our final analysis, presented in this Appendix, we adapted the PHENIX method for comparison of a dataset that contains data with errors directly to another dataset, that also contains central data values with errors. So our method is defined without referring to any theoretical model or parameter dependent function. Due to this reason, the most conservative definition described in this Appendix is defined to be *symmetric for the exchange of the two datasets*.

We classify the experimental errors of a given data set into three different types: (i) type A, point-to-point fluctuating (uncorrelated) systematic and statistical errors, (ii) type B errors that are point-to-point dependent, but 100% correlated systematic errors, and (iii) type C errors, that are point-to-point independent, but fully correlated systematic errors [70] to evaluate the significance of correlated data, when the covariance matrix is not publicly available.

Suitably generalizing the method of Ref. [70] for a comparison of two data sets in this case, we obtain the significance of a projection of the data set  $D_2$  to data set  $D_1$  determined by the following  $\chi^2$  definition:

$$\tilde{\chi}_{21}^2 = \sum_{j=1}^{n_{21}} \frac{(d_1(j) + \varepsilon_{b,1} e_{B,1}(j) - d_{21}(j) - \varepsilon_{b,21} e_{B,21}(j))^2}{\tilde{\varepsilon}_{A,1}^2(j) + \tilde{\varepsilon}_{A,21}^2(j)} + \varepsilon_{b,1}^2 + \varepsilon_{b,21}^2. \quad (\text{A.1})$$

In this equation,  $\tilde{\varepsilon}_{A,1}(j)$  is the type A uncertainty of the data point  $j$  of the data set  $D_1$  in the united acceptance, while  $\tilde{\varepsilon}_{A,21}(j)$  is the same for the  $D_{21}$  data set obtained from the  $D_2$  dataset by interpolation to point  $j$  of dataset  $D_1$ . Both uncertainties are scaled by a multiplicative factor such that



the fractional uncertainty is unchanged under multiplication by a point-to-point varying factor:

$$\tilde{e}_{A,1}(j) = e_{A,1}(j) \left( \frac{d_1(j) + \varepsilon_{b,1} e_{B,1}(j)}{d_1(j)} \right), \quad (\text{A.2})$$

$$\tilde{e}_{A,21}(j) = e_{A,21}(j) \left( \frac{d_{21}(j) + \varepsilon_{b,21} e_{B,21}(j)}{d_{21}(j)} \right). \quad (\text{A.3})$$

In these equations,  $\varepsilon_{b,1}$  and  $\varepsilon_{b,21}$  stand for the overall correlation coefficient of the  $j$ -dependent, point-to-point correlated type B  $D_2$  to the measured values in data set  $D_1$ ,  $e_{B,21}(j)$  of the projected data set  $D_{21}$ . Note that  $\varepsilon_{b,1}$  and  $\varepsilon_{b,21}$  are independent of the point  $j$ , while the B-type errors have a point-to-point changing values  $e_{B,1}(j)$  and  $e_{B,21}(j)$  in both  $D_1$  and in the projected dataset in  $D_{21}$ . For our comparison of  $H(x)$  scaling functions, where the absolute normalization and type C errors cancel, we have  $\varepsilon_{c,1} = \varepsilon_{c,2} = 0$ , so have not indicated these terms for the sake of simplicity.

We have utilized the scaled variance method of ROOT to include the horizontal errors, adding in quadrature the type A errors also the type A error coming from the type A uncertainty of  $x$ , denoted as  $\delta_A x$ . Similarly, we have added in quadrature the type B error of the type B uncertainty of  $x$ , denoted by  $\delta_B x$ . Using a notation where  $M$  may stand for any of A or B, the errors are given as

$$e_{M,1}^2(j) = \sigma_{M,1}^2(j) + [d'_1(j) \delta_{M,1} x(j)]^2, \quad (\text{A.4})$$

$$e_{M,21}^2(j) = \sigma_{M,21}^2(j) + [d'_{21}(j) \delta_{M,21} x(j)]^2, \quad (\text{A.5})$$

where  $\sigma_M(j)$  indicates the type  $M \in \{A, B\}$  error of the value of the vertical error on data point  $j$ , and it is added in quadrature with  $d'(j) \delta_M x(j)$ , the corresponding vertical error that is associated with the same uncertainty of type  $M$  originating from the measurement error on the horizontal axis  $x$  in Eq. (A.4). The notations  $d'_1(j)$  and  $d'_{21}(j)$  stand for the numerical derivative of the data points at point  $j$  in the datasets  $D_1$  and  $D_{21}$ , respectively.

The errors on the projected data set ( $D_{21}$ ) are also obtained by a linear-exponential interpolation between the projections of data set 2 ( $D_2$ ) to data set 1 ( $D_1$ ). Their type A and type B errors, indicated by  $e_{A,21}(j)$  and  $e_{B,21}(j)$  are also added in quadrature with the other A or B type of errors. These errors on the interpolated and on the measured values of  $(x, H(x))$  through equations (A.4) and (A.5) provided our most stringent significance estimate for the Odderon effects. We have cross-checked that several variations on the  $\chi^2$  definition, for example the frequently adopted neglect of the horizontal errors and their contribution to the vertical errors through the scaled variance method, or perturbing the central values or the errors of the elastic cross-sections within the allowed limits, may only increase the significance reported in this Appendix.

We have evaluated Eq. (62) as a function of  $\varepsilon_{b,1}$  and  $\varepsilon_{b,21}$ . However, for the critical test of the projection of the  $\sqrt{s} = 7.0$  TeV TOTEM data on  $H(x)$  to that of D0 at  $\sqrt{s} =$

1.96 TeV, we found that D0 did not publish any error on  $-t$  and cross-checked that the D0 value on  $B$  contains only type A, uncorrelated statistical and systematic errors only. We also noticed that there are no published type-B errors on the published differential cross-section data of D0 [8]. Hence for the D0 dataset, all the type B errors are zero and as a consequence, we have fixed the correlation coefficient of type B errors to zero for the  $\sqrt{s} = 1.96$  TeV D0 dataset.

Let us now denote by subscript 21 the projection of the  $H(x)$  scaling function at  $\sqrt{s} = 7$  TeV measured by TOTEM for  $pp$  reaction to the D0 dataset on  $p\bar{p}$  elastic scattering at  $\sqrt{s} = 1.96$  TeV. We found a minimum for  $\varepsilon_{b,21} \equiv \varepsilon_{b,7\text{TeV}}$  within the  $-1 \leq \varepsilon_{b,21} \leq 1$  domain, with the best value of  $\varepsilon_{b,7\text{TeV}}$  and the lowest value of  $\chi^2 \equiv \tilde{\chi}_{21}^2$  of eq. (A.1) indicated on Fig. 13. Table 6 summarizes the input values and the appropriate references to the utilized elastic cross-section  $\sigma_{\text{el}}$  and the nuclear slope  $B(s)$ . The final and most stringent result of this cross check, corresponding to the lowest values of significance for the Odderon observation is summarized in Table 7. We found that the significance of the Odderon observation in the 7 TeV  $\rightarrow$  1.96 TeV projection is at least  $6.26\sigma$ , corresponding to a  $\chi^2/\text{NDF} = 80.1/17$  and CL of not larger than  $3.7 \times 10^{-8} \%$ . We notice that all variations of the procedure may only increase this significance. We conclude that the probability of the Odderon observation in this  $t$ -channel mode is statistically significant, at least  $P = 1 - \text{CL} = 0.99999999963$ .

## Acknowledgments

We acknowledge inspiring discussions with C. Avila, S. Gi-ani, P. Grannis, W. Guryn, G. Gustafson, V. A. Khoze, E. Levin, L. Lönnblad, K. Österberg, C. Royon, M. Strikman and M. Šumbera. We thank our Referee for valuable comments, suggestions and clarifications, in particular for suggesting to create an easier-to-read summary of these results, that we have provided in ref. [68]. R.P. is partially supported by the Swedish Research Council grants No. 621-2013-4287 and 2016-05996, by the European Research Council (ERC) under the European Union's Horizon 2020 research and innovation programme (grant agreement No 668679), as well as by the Ministry of Education, Youth and Sports of the Czech Republic project LTT17018 and by the NKFI grant K133046 (Hungary). T. Cs, T. N, I. Sz. and A. S. were partially supported by the NKFIH grants No. FK-123842, FK-123959 and K133046 as well as by the EFOP 3.6.1-16-2016-00001 grant (Hungary). Our collaboration was supported by the framework of COST Action CA15213 "Theory of hot matter and relativistic heavy-ion collisions" (THOR).

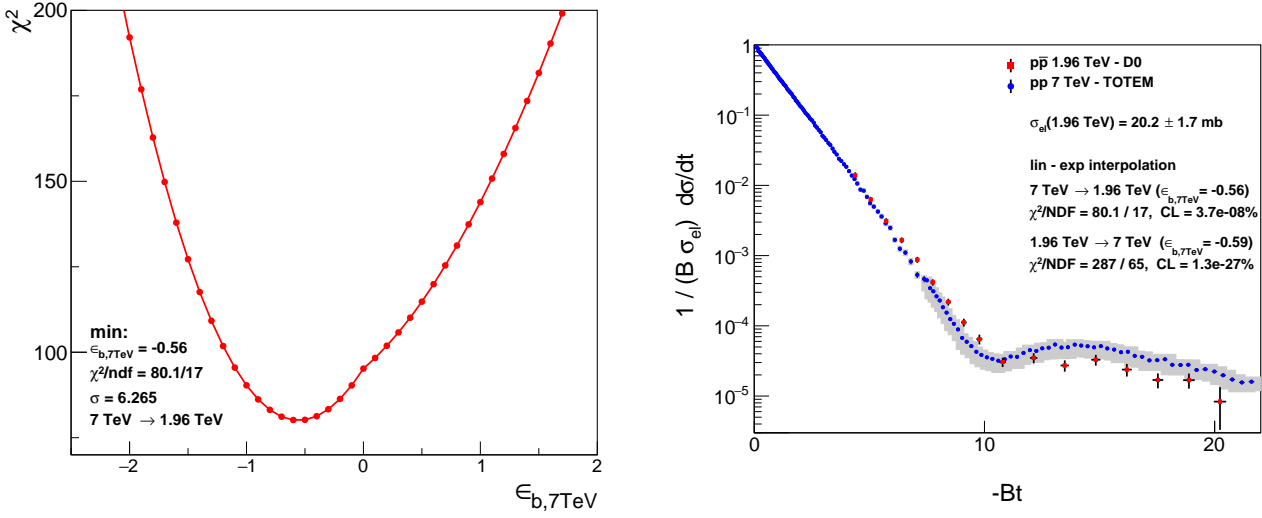


**Fig. 13** Left panel indicates that as a function of  $\epsilon_{b,7 \text{ TeV}}$ , the  $\chi^2 \equiv \tilde{\chi}_{21}^2$  distribution has a unique minimum and nearly quadratic minimum. The minimum value is  $\chi^2/\text{NDF} = 80.1/17$ , corresponding to a statistically significant difference between the  $pp$  and  $p\bar{p}$   $H(x)$  scaling functions, at the level of  $6.26\sigma$ . The right panel shows the comparison of the  $H(x)$  data using the values of  $\epsilon_{b,7 \text{ TeV}}$  corresponding to such a minimum, both for the case of the  $7 \rightarrow 1.96 \text{ TeV}$  and for the case of  $1.96 \rightarrow 7 \text{ TeV}$  projections.

$\sqrt{s}$ (GeV)	$\sigma_{\text{el}}$ (mb)	$B$ (GeV $^{-2}$ )
1960 ( $p\bar{p}$ )	$20.2 \pm 1.7^A \pm 14.4\%^C$ [*]	$16.86 \pm 0.1^A \pm 0.2^A$ [8]
2760 ( $pp$ )	$21.8 \pm 1.4^A \pm 6.0\%^C$ [4, 45]	$17.1 \pm 0.3^A$ [4]
7000 ( $pp$ )	$25.43 \pm 0.03^A \pm 0.1^B \pm 0.31^C \pm 1.02^C$ [28]	$19.89 \pm 0.03^A \pm 0.27^B$ [28]

**Table 6** Summary table of the elastic cross-sections  $\sigma_{\text{el}}$ , the nuclear slope parameters  $B$ , with references. We have indexed with superscript A the type A, point-to-point fluctuating systematic and statistical errors, that can be added in quadrature, while type B errors (point-to-point changing, fully correlated systematic errors) are indicated with superscript B and type C errors (overall correlated, but  $-t$  independent errors) are indicated with superscript C. Note that the value and the type A error of the elastic cross-section  $\sigma_{\text{el}}$  at  $\sqrt{s} = 1.96 \text{ TeV}$  [\*] is obtained from a low  $-t$  exponential fit to data of Ref. [8], while the type C error is directly taken from the publication [8].

$\sigma_{\text{el}}$ (mb)	interpolation	direction of projection	$\chi^2$	NDF	CL (%)	Significance [ $\sigma$ ]
$20.2 \pm 1.7$	lin-exp	$7 \rightarrow 1.96 \text{ TeV}$	80.1	17	$3.7 \times 10^{-8}$	6.26

**Table 7** Summary table of the significant Odderon signal in the one-way comparison of the  $H(x)$  scaling functions of proton-proton collisions at  $\sqrt{s} = 7 \text{ TeV}$ , as measured by the TOTEM experiment at CERN LHC [28, 69], and proton - antiproton elastic collisions at  $\sqrt{s} = 1.96 \text{ TeV}$  as measured by the D0 experiment at Tevatron [8]. This table indicates that the Odderon signal is observed in this comparison with at least a  $6.26 \sigma$  significance, corresponding to an Odderon discovery.

## References

1. **TOTEM** Collaboration, G. Antchev *et al.*, “First measurement of elastic, inelastic and total cross-section at  $\sqrt{s} = 13 \text{ TeV}$  by TOTEM and overview of cross-section data at LHC energies,” *Eur. Phys. J. C* **79** no. 2, (2019) 103, [arXiv:1712.06153 \[hep-ex\]](#).
2. **TOTEM** Collaboration, G. Antchev *et al.*, “First determination of the  $\rho$  parameter at  $\sqrt{s} = 13 \text{ TeV}$  – probing the existence of a colourless three-gluon bound state,” [arXiv:1812.04732 \[hep-ex\]](#).
3. **TOTEM** Collaboration, G. Antchev *et al.*, “Elastic differential cross-section measurement at  $\sqrt{s} = 13 \text{ TeV}$  by TOTEM,” [arXiv:1812.08283 \[hep-ex\]](#).
4. **TOTEM** Collaboration, G. Antchev *et al.*, “Elastic differential cross-section  $d\sigma/dt$  at  $\sqrt{s} = 2.76 \text{ TeV}$  and implications on the existence of a colourless 3-gluon bound state,” [arXiv:1812.08610 \[hep-ex\]](#).
5. A. P. Samokhin and V. A. Petrov, “The Stationary Points and Structure of High-Energy Scattering Amplitude,” *Nucl. Phys.* **A974** (2018) 45–55, [arXiv:1708.02879 \[hep-ph\]](#).
6. V. A. Khoze, A. D. Martin, and M. G. Ryskin, “Elastic and diffractive scattering at the LHC,” *Phys. Lett.* **B784** (2018) 192–198, [arXiv:1806.05970 \[hep-ph\]](#).

7. L. Lukaszuk and B. Nicolescu, “A Possible interpretation of  $p\,p$  rising total cross-sections,” *Lett. Nuovo Cim.* **8** (1973) 405–413.
8. **D0** Collaboration, V. M. Abazov *et al.*, “Measurement of the differential cross section  $d\sigma/dt$  in elastic  $p\bar{p}$  scattering at  $\sqrt{s} = 1.96$  TeV,” *Phys. Rev.* **D86** (2012) 012009, [arXiv:1206.0687 \[hep-ex\]](#).
9. T. Csörgő, R. Pasechnik, and A. Ster, “Odderon and proton substructure from a model-independent Lévy imaging of elastic  $pp$  and  $p\bar{p}$  collisions,” *Eur. Phys. J. C* **79** no. 1, (2019) 62, [arXiv:1807.02897 \[hep-ph\]](#).
10. A. Ster, L. Jenkovszky, and T. Csörgő, “Extracting the Odderon from  $pp$  and  $p\bar{p}$  scattering data,” *Phys. Rev.* **D91** no. 7, (2015) 074018, [arXiv:1501.03860 \[hep-ph\]](#).
11. V. P. Gonçalves and P. V. R. G. Silva, “The Phillips–Barger model for the elastic cross section and the Odderon,” *Eur. Phys. J. C* **79** no. 3, (2019) 237, [arXiv:1811.12250 \[hep-ph\]](#).
12. V. A. Khoze, A. D. Martin, and M. G. Ryskin, “Elastic proton-proton scattering at 13 TeV,” *Phys. Rev.* **D97** no. 3, (2018) 034019, [arXiv:1712.00325 \[hep-ph\]](#).
13. O. Selyugin and J. Cudell, “Odderon, HEGS model and LHC data,” *Acta Phys. Polon. Supp.* **12** no. 4, (2019) 741, [arXiv:1810.11538 \[hep-ph\]](#).
14. M. Broilo, E. G. S. Luna, and M. J. Menon, “Soft Pomerons and the Forward LHC Data,” *Phys. Lett.* **B781** (2018) 616–620, [arXiv:1803.07167 \[hep-ph\]](#).
15. M. Broilo, E. G. S. Luna, and M. J. Menon, “Forward Elastic Scattering and Pomeron Models,” *Phys. Rev.* **D98** no. 7, (2018) 074006, [arXiv:1807.10337 \[hep-ph\]](#).
16. T. Csörgő, R. Pasechnik, and A. Ster, “Proton structure and hollowness from Lévy imaging of  $pp$  elastic scattering,” *Eur. Phys. J. C* **80** no. 2, (2020) 126, [arXiv:1910.08817 \[hep-ph\]](#).
17. S. M. Troshin and N. E. Tyurin, “Implications of the  $\rho(s)$  measurements by TOTEM at the LHC,” *Mod. Phys. Lett. A* **33** no. 35, (2018) 1850206, [arXiv:1805.05161 \[hep-ph\]](#).
18. E. Gotsman, E. Levin, and I. Potashnikova, “CGC/saturation approach: secondary Reggeons and  $\rho = \text{Re}/\text{Im}$  dependence on energy,” *Phys. Lett.* **B786** (2018) 472–476, [arXiv:1807.06459 \[hep-ph\]](#).
19. E. Gotsman, E. Levin, and I. Potashnikova, “A new parton model for the soft interactions at high energies: the Odderon,” [arXiv:2003.09155 \[hep-ph\]](#).
20. Y. Hagiwara, Y. Hatta, R. Pasechnik, and J. Zhou, “Spin-dependent Pomeron and Odderon in elastic proton-proton scattering,” [arXiv:2003.03680 \[hep-ph\]](#).
21. C. Contreras, E. Levin, R. Meneses, and M. Sanhueza, “QCD Odderon: non linear evolution in the leading twist,” [arXiv:2004.04445 \[hep-ph\]](#).
22. E. Martynov and B. Nicolescu, “Evidence for maximality of strong interactions from LHC forward data,” *Phys. Lett.* **B786** (2018) 207–211, [arXiv:1804.10139 \[hep-ph\]](#).
23. E. Martynov and B. Nicolescu, “Odderon effects in the differential cross-sections at Tevatron and LHC energies,” *Eur. Phys. J. C* **79** no. 6, (2019) 461, [arXiv:1808.08580 \[hep-ph\]](#).
24. Y. M. Shabelski and A. G. Shuvaev, “Real part of  $pp$  scattering amplitude in Additive Quark Model at LHC energies,” *Eur. Phys. J. C* **78** no. 6, (2018) 497, [arXiv:1802.02812 \[hep-ph\]](#).
25. G. Pancheri, S. Pacetti, and Y. Srivastava, “Analysis and Implications of precision near-forward TOTEM data,” *Phys. Rev. D* **99** no. 3, (2019) 034014, [arXiv:1811.00499 \[hep-ph\]](#).
26. T. Csörgő, R. Pasechnik, and A. Ster, “Model-independent femtoscopic Lévy imaging for elastic proton-proton scattering,” [arXiv:1811.08913 \[hep-ph\]](#).
27. T. Csörgő, R. Pasechnik, and A. Ster, “Lévy imaging of elastic hadron-hadron scattering: Odderon and inner structure of the proton,” in *Diffraction and Low- $x$  2018 (Diffloxx2018) Reggio Calabria, Italy, August 26-September 1, 2018*. 2019. [arXiv:1902.00109 \[hep-ph\]](#).
28. **TOTEM** Collaboration, G. Antchev *et al.*, “Measurement of proton-proton elastic scattering and total cross-section at  $\sqrt{s} = 7$  TeV,” *EPL* **101** no. 2, (2013) 21002.
29. W. Broniowski, L. Jenkovszky, E. Ruiz Arriola, and I. Szanyi, “Hollowness in  $pp$  and  $p\bar{p}$  scattering in a Regge model,” *Phys. Rev.* **D98** no. 7, (2018) 074012, [arXiv:1806.04756 \[hep-ph\]](#).
30. A. Bialas and A. Bzdak, “Constituent quark and diquark properties from small angle proton-proton elastic scattering at high energies,” *Acta Phys. Polon.* **B38** (2007) 159–168, [arXiv:hep-ph/0612038 \[hep-ph\]](#).
31. F. Nemes and T. Csörgő, “Detailed Analysis of  $p^+p$  Elastic Scattering Data in the Quark-Diquark Model of Bialas and Bzdak from  $\sqrt{s} = 23.5$  GeV to 7 TeV,” *Int. J. Mod. Phys. A* **27** (2012) 1250175, [arXiv:1204.5617 \[hep-ph\]](#).
32. T. Csörgő and F. Nemes, “Elastic scattering of protons from  $\sqrt{s} = 23.5$  GeV to 7 TeV from a generalized Bialas-Bzdak model,” *Int. J. Mod. Phys. A* **29** (2014) 1450019, [arXiv:1306.4217 \[hep-ph\]](#).

33. F. Nemes, T. Csörgő, and M. Csanád, “Excitation function of elastic pp scattering from a unitarily extended Bialas–Bzdak model,” *Int. J. Mod. Phys. A* **30** no. 14, (2015) 1550076, [arXiv:1505.01415 \[hep-ph\]](#).
34. V. Petrov and A. Samokhin, “Is There a Hollow Inside the Proton?,” *Int. J. Mod. Phys. Conf. Ser.* **47** (2018) 1860097, [arXiv:1801.03809 \[hep-ph\]](#).
35. I. M. Dremin and V. A. Nechitailo, “Proton periphery activated by multiparticle dynamics,” *Nucl. Phys. A* **916** (2013) 241–248, [arXiv:1306.5384 \[hep-ph\]](#).
36. I. M. Dremin, “Interaction region of high energy protons,” *Phys. Usp.* **58** no. 1, (2015) 61–70, [arXiv:1406.2153 \[hep-ph\]](#).
37. I. M. Dremin and V. A. Nechitailo, “Inelastic profiles of protons at 7 and 13 TeV,” *Eur. Phys. J. C* **78** no. 11, (2018) 913.
38. I. Dremin, “Cul-De-Sac of the Spatial Image of Proton Interactions,” *MDPI Physics* **1** no. 1, (2019) 33–39.
39. L. L. Jenkovszky, A. I. Lengyel, and D. I. Lontkovskyi, “The Pomeron and Odderon in elastic, inelastic and total cross sections at the LHC,” *Int. J. Mod. Phys. A* **26** (2011) 4755–4771, [arXiv:1105.1202 \[hep-ph\]](#).
40. R. J. N. Phillips and V. D. Barger, “Model independent analysis of the structure in p p scattering,” *Phys. Lett.* **46B** (1973) 412–414.
41. P. Lebiedowicz, O. Nachtmann, and A. Szczurek, “Towards a complete study of central exclusive production of  $K^+K^-$  pairs in proton-proton collisions within the tensor Pomeron approach,” *Phys. Rev. D* **98** (2018) 014001, [arXiv:1804.04706 \[hep-ph\]](#).
42. TOTEM Collaboration, T. Csörgő, “Recent Results from the CERN LHC Experiment TOTEM – Implications for Odderon Exchange,” *EPJ Web Conf.* **206** (2019) 06004, [arXiv:1903.06992 \[hep-ex\]](#).
43. M. M. Block, “Hadronic forward scattering: Predictions for the Large Hadron Collider and cosmic rays,” *Phys. Rept.* **436** (2006) 71–215, [arXiv:hep-ph/0606215 \[hep-ph\]](#).
44. D. A. Fagundes and M. J. Menon, “Total Hadronic Cross Section and the Elastic Slope: An Almost Model-Independent Connection,” *Nucl. Phys. A* **880** (2012) 1–11, [arXiv:1112.5115 \[hep-ph\]](#).
45. F. J. Nemes, “Elastic and total cross-section measurements by TOTEM: Past and future,” *PoS DIS2017* (2018) 059.
46. TOTEM Collaboration, G. Antchev *et al.*, “Luminosity-independent measurements of total, elastic and inelastic cross-sections at  $\sqrt{s} = 7$  TeV,” *EPL* **101** no. 2, (2013) 21004.
47. TOTEM Collaboration, G. Antchev *et al.*, “Luminosity-Independent Measurement of the Proton-Proton Total Cross Section at  $\sqrt{s} = 8$  TeV,” *Phys. Rev. Lett.* **111** no. 1, (2013) 012001.
48. S. M. Troshin and N. E. Tyurin, “Reflective scattering from unitarity saturation,” *Int. J. Mod. Phys. A* **22** (2007) 4437–4449, [arXiv:hep-ph/0701241 \[hep-ph\]](#).
49. A. Alkin, E. Martynov, O. Kovalenko, and S. M. Troshin, “Impact-parameter analysis of TOTEM data at the LHC: Black disk limit exceeded,” *Phys. Rev. D* **89** no. 9, (2014) 091501, [arXiv:1403.8036 \[hep-ph\]](#).
50. S. M. Troshin and N. E. Tyurin, “Effects of the reflective scattering in hadron production at high energies,” *Int. J. Mod. Phys. A* **29** no. 26, (2014) 1450151, [arXiv:1408.2650 \[hep-ph\]](#).
51. V. V. Anisovich, V. A. Nikonov, and J. Nyiri, “Hadron collisions at ultrahigh energies: black disk or resonant disk modes?,” *Phys. Rev. D* **90** no. 7, (2014) 074005, [arXiv:1408.0692 \[hep-ph\]](#).
52. E. Ruiz Arriola and W. Broniowski, “Proton-proton hollowness at the LHC from inverse scattering,” *Phys. Rev. D* **95** no. 7, (2017) 074030, [arXiv:1609.05597 \[nucl-th\]](#).
53. S. M. Troshin and N. E. Tyurin, “The new scattering mode emerging at the LHC?,” *Mod. Phys. Lett. A* **31** no. 13, (2016) 1650079, [arXiv:1602.08972 \[hep-ph\]](#).
54. J. L. Albacete and A. Soto-Ontoso, “Hot spots and the hollowness of proton–proton interactions at high energies,” *Phys. Lett. B* **770** (2017) 149–153, [arXiv:1605.09176 \[hep-ph\]](#).
55. W. Broniowski and E. Ruiz Arriola, “Hollowness in pp scattering,” *Acta Phys. Polon. B* **48** (2017) 927, [arXiv:1704.03271 \[hep-ph\]](#).
56. W. Broniowski and E. Ruiz Arriola, “Hollowness in pp scattering at the LHC,” *Acta Phys. Polon. Supp.* **10** (2017) 1203, [arXiv:1708.00402 \[nucl-th\]](#).
57. S. M. Troshin and N. E. Tyurin, “Experimental signatures of hadron asymptotics at the LHC,” *Int. J. Mod. Phys. A* **32** no. 17, (2017) 1750103, [arXiv:1704.00443 \[hep-ph\]](#).
58. I. M. Dremin, “Some new discoveries at colliders,” *Usp. Fiz. Nauk* **188** no. 4, (2018) 437–445. [*Phys. Usp.* 61,no.4,381(2018)].
59. S. D. Campos and V. A. Okorokov, “Hollowness effect and entropy in high energy elastic scattering,” [arXiv:1807.02061 \[hep-ph\]](#).
60. J. Dias De Deus, “Geometric Scaling, Multiplicity Distributions and Cross-Sections,” *Nucl. Phys. B* **59** (1973) 231–236.
61. A. J. Buras and J. Dias de Deus, “Scaling law for the elastic differential cross-section in p p scattering from geometric scaling,” *Nucl. Phys. B* **71** (1974) 481–492.
62. U. Amaldi and K. R. Schubert, “Impact Parameter Interpretation of Proton Proton Scattering from a

- Critical Review of All ISR Data,” *Nucl. Phys.* **B166** (1980) 301–320.
63. **TOTEM** Collaboration, G. Antchev *et al.*, “Evidence for non-exponential elastic proton–proton differential cross-section at low  $|t|$  and  $\sqrt{s}=8$  TeV by TOTEM,” *Nucl. Phys. B* **899** (2015) 527–546, [arXiv:1503.08111 \[hep-ex\]](#).
  64. **TOTEM** Collaboration, T. Csörgő, “Evidence for Non-Exponential Differential Cross-Section of pp Elastic Scattering at Low  $|t|$  and  $\sqrt{s} = 8$  TeV by TOTEM,” *EPJ Web Conf.* **120** (2016) 02004, [arXiv:1602.00219 \[hep-ex\]](#).
  65. T. Csörgő, S. Hegyi, and W. Zajc, “Bose-Einstein correlations for Levy stable source distributions,” *Eur. Phys. J. C* **36** (2004) 67–78, [arXiv:nucl-th/0310042](#).
  66. A. K. Kohara, E. Ferreira, T. Kodama, and M. Rangel, “Elastic amplitudes studied with the LHC measurements at 7 and 8 TeV,” *Eur. Phys. J. C* **77** no. 12, (2017) 877, [arXiv:1709.05713 \[hep-ph\]](#).
  67. J. Kaspar, “Soft diffraction at LHC,” *EPJ Web of Conferences* **172** (2018) 06005. <https://doi.org/10.1051/epjconf/201817206005>.
  68. T. Csörgő, T. Novák, R. Pasechnik, A. Ster, and I. Szanyi, “Scaling of high-energy elastic scattering and the observation of Odderon,” [arXiv:2004.07318 \[hep-ph\]](#).
  69. **TOTEM** Collaboration, G. Antchev *et al.*, “Proton-proton elastic scattering at the LHC energy of  $s^{**}(1/2) = 7$ -TeV,” *EPL* **95** no. 4, (2011) 41001, [arXiv:1110.1385 \[hep-ex\]](#).
  70. **PHENIX** Collaboration, A. Adare *et al.*, “Quantitative Constraints on the Opacity of Hot Partonic Matter from Semi-Inclusive Single High Transverse Momentum Pion Suppression in Au+Au collisions at  $s(NN)^{**}(1/2) = 200$ -GeV,” *Phys. Rev. C* **77** (2008) 064907, [arXiv:0801.1665 \[nucl-ex\]](#).
  71. **Particle Data Group** Collaboration, M. Tanabashi *et al.*, “Review of Particle Physics,” *Phys. Rev.* **D98** no. 3, (2018) 030001.